Chem Soc Rev

The springtail cuticle as a blueprint for omniphobic surfaces

Journal:	*Chemical Society Reviews*
Manuscript ID:	CS-REV-05-2015-000438.R2
Article Type:	Review Article
Date Submitted by the Author:	24-Jul-2015
Complete List of Authors:	Hensel, René; INM - Leibniz Institute for New Materials, Functional Microstructures Neinhuis, Christoph; Technische Universität Dresden, Institute of Botany Werner, Carsten; Leibniz Institute of Polymer Research Dresden, Max Bergmann Center of Biomaterials Dresden

The springtail cuticle as a blueprint for omniphobic surfaces

René Hensel[a], Christoph Neinhuis[b,d] and Carsten Werner*[c,d]

[a] INM – Leibniz Institute for New Materials, 66123 Saarbrücken, Germany
[b] Institute of Botany, Technische Universität Dresden, 01062 Dresden, Germany
[c] Max Bergmann Center of Biomaterials, Leibniz Institute of Polymer Research Dresden, 01069 Dresden, Germany
[d] B CUBE Innovation Center for Molecular Bioengineering, Technische Universität Dresden, 01307 Dresden, Germany

*Corresponding author: Email: werner@ipfdd.de

Abstract

Omniphobic surfaces found in nature have great potential for enabling novel and emerging products and technologies to facilitate the daily life of human societies. One example is the water and even oil-repellent cuticle of springtails (Collembola). The wingless arthropods evolved a highly textured, hierarchically arranged surface pattern that affords mechanical robustness and wetting resistance even at elevated hydrostatic pressures. Springtail cuticle-derived surfaces therefore promise to overcome limitations of lotus-inspired surfaces (low durability, insufficient repellence of low surface tension liquids). In this review, we report on the liquid-repellent natural surfaces of arthropods living in aqueous or temporarily flooded habitats including water-walking insects or water spiders. In particular, we focus on springtails presenting an overview on the cuticular morphology and chemistry and their biological relevance. Based on the obtained liquid repellence of a variety of liquids with remarkable efficiency, the review provides general design criteria for robust omniphobic surfaces. In particular, the resistance against complete wetting and the mechanical stability strongly both depend on the topographical features of the nano- and micropatterned surface. The current understanding of the underlying principles and approaches to their technological implementation are summarized and discussed.

TOC Graphic

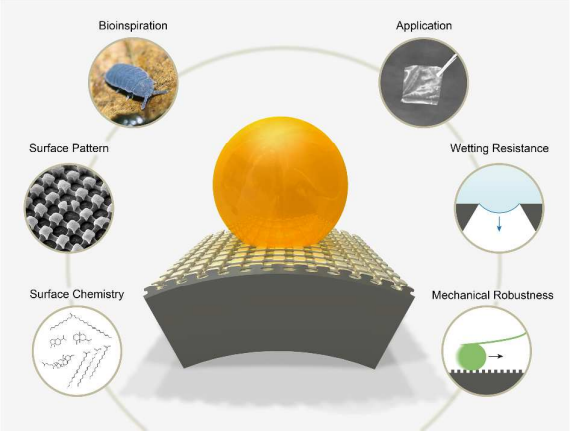

Robust omniphobic surface coatings inspired by the cuticular structure of springtails (Collembola).

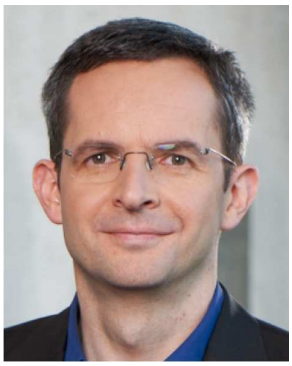

Carsten Werner

Carsten Werner is professor for Biofunctional Polymer Materials at TU Dresden and deputy director of the Leibniz Institute for Polymer Research Dresden, Germany (IPF). His research interests include electrosurface phenomena, hemocompatible materials, cell-instructive polymer matrices for regenerative therapies and biomimicry concepts in materials science. Carsten Werner holds an Adjunct Full Professorship at the Institute of Biomaterials and Biomedical Engineering of the University of Toronto, Ontario, Canada, and serves as Associate Editor of Biomaterials and Section Editor of Current Opinion in Colloid and Interface Science. He has authored or co-authored more than 250 publications and filed more than 30 patents.

Christoph Neinhuis

Christoph Neinhuis holds the chair for botany at TU Dresden. He is also director of the Botanical Garden, and from 2006 to 2012 he was appointed Speaker of the Department of Biology. Research interests cover plant biodiversity, especially systematics and phylogeny of Aristolochiaceae and Piperaceae as well as biomechanics and functional morphology. Long lasting research interest counted for non-wettable and self-cleaning biomimetic surfaces, which was awarded by the Philipp-Morris Foundation. Recently he concentrated on fiber-based plant structures and their potential for composites in engineering.

René Hensel

Dr. René Hensel studied materials science at the TU Dresden, Germany. He was a fellow of the DFG Research Training Group 1401/2 at the TU Dresden and did his doctorate at the Leibniz Institute of Polymer Research Dresden (IPF) and the Max Bergmann Center of Biomaterials Dresden (MBC). He has obtained the International Bionic Award 2014 from VDI for his PhD thesis on free-standing polymer membranes for omniphobic and mechanically stable surface coatings. Since 2014, he has been deputy head of the Program Division Functional Microstructures at Leibniz Institute for New Materials Saarbrücken, Germany.

1. Introduction

Hierarchically-assembled natural surfaces can be the origin of exciting and unique physical effects such as liquid-repellence, self-cleaning, drag reduction in hydrodynamic flow, anti-icing, energy conversion and conservation, high, low or reversible adhesion, non-fouling, structural coloration and so on.[1–7] These surfaces typically represent the interface between an organism and its environment where various physical, chemical, and biological reactions and processes take place.[8–11] As a consequence, natural surfaces often have to fulfill several functions, which are achieved by complex morphologies and chemical compositions as a result of adaption and optimization by evolutionary processes.[12–15] Mimicking natural surfaces is an appropriate strategy to translate (at least one) characteristic physical effect into synthetic materials, which would offer exciting opportunities for emerging applications.[16–21]

Probably, one of the famous examples of nature-inspired concepts is the water-repellent cuticular surface of the sacred lotus, which exhibits self-cleaning properties known nowadays as the Lotus-Effect (**Figure 1A-D**). The effect is based on rough hydrophobic waxes covering the leaf that reduce the contact area as well as the adhesion of dust particles and water droplets. As a result, rolling water droplets easily capture dust particles from the surface due to their higher attraction to the liquid than to the solid.[22,23] Such repellent and self-cleaning surfaces can be useful in numerous technological processes and products, especially by reducing expensive cleaning procedures or lengthening cleaning intervals. In the 1970s, Barthlott discovered this characteristic behavior while he was exploring the nano- and microscopic surface features of plants, particularly, the epicuticular wax crystals.[24,25] In nature, the self-cleaning phenomenon is necessary for sufficient photosynthesis and relates to a defense mechanism against potentially dangerous pathogens such as bacteria and fungi.[5,21,26]

In addition to the self-cleaning capabilities, water-repelling surfaces in nature can further facilitate walking on water by trapping air inside bunches of micro-setae that cover the legs of semi-aquatic arthropods such as water striders (**Figure 1E-H**).[27,28] Feng *et al*. reported that the maximal buoyant force exerted by the water strider is 60 times higher than its body weight.[29] The entrapped air pockets between the legs and the water surface afford the ability to float and reduce the drag; however, it counteracts the propulsion ability.[30] Hu *et al*. revealed that water striders move by rowing using the legs as paddles and the menisci as blades, whereas the momentum is transferred through subsurface vortices.[31,32] Furthermore, the anisotropic wetting behavior of the inclined setae pointing towards the leg tips enhances the propulsion force.[33]

The ability to trap air by water-repellent surfaces allows several aquatic and semi-aquatic arthropods to respire under water upon complete immersion, as known from the fisher spider *Dolomedes triton* or the backswimmer *Notonecta*. The trapped air reservoir acts as a gill under water and is referred to as a plastron.[34] The gas transfer rate by diffusion is much higher in air than in water. Therefore, most of the arthropods living in aqueous habitats or temporarily flooded environments exhibit water-repelling openings of their tracheal networks.[35–37] For aquatic plants, the trapped air provides a higher metabolic rate by photosynthesis again due to the better diffusion of CO_2 in air than in water.[38] An even more striking example of trapping air under water is the aquatic fisher spider *Argyroneta aquatica*.[39,40] The spider lives its entire life under water but needs air to breathe. To survive

under water, the spider permanently collects air from the water surface and feeds its diving bell that is immobilized between aquatic plants and a dome-shaped web. To collect the air, the rear part of the spider is covered by a mat of non-wetting hairs that help to trap and carry air bubbles into the water and down to the diving bell (**Figure 1J-L**).

Before translating such a phenomenon into engineered surfaces, the fundamental physicochemical principles behind such phenomena have to be understood, i.e., the common pathway in biomimetics.[41] As an example, the surface morphology and chemistry of the lotus leaf was intensively studied over the past two decades and inspired engineers to manufacture water-repellent surfaces with a broad scope of applications.[19,42–44] It was found that both the surface chemistry and the morphology, in particular, the hierarchical structure of the surface are crucial for water repellence.[45,46] Nevertheless, an abstraction into simplified, non-hierarchical structures such as needle-like nanostructures or microscopic bulb or pillar structures in combination with low-surface-energy coatings such fluoropolymers or hydrocarbons also addresses a water-repellent characteristic in a preliminary manner as depicted in **Figure 2**.[10,47] Non-hierarchical structures are in turn easier to fabricate than sophisticated hierarchical structures using common micromanufacturing processes such as lithography, etching, deposition, sol-gel or replication techniques.[16,47,48] However, the abstraction into needle or pillar structures entails a serious list of drawbacks:

1. The repellence is often restricted to aqueous media and fails for liquids with lower surface tensions such as oils or water containing surfactants.[49]
2. The energetic barrier against complete wetting, i.e., the loss of repellence, of the surface is often even less than the kinetic energy of falling rain droplets and, thus, the structures are neither applicable for outdoor coatings nor suitable for large immersion depths.[50,51]
3. The inherent fragility of the tiny surface features limits the resistance to shear-loads, e.g., by scratching.[22,52,53]

So far, these points represent the main limitations that significantly impede a broad range of applications.[54] Several experimental and theoretical studies induced concepts on how to design the surface features to improve certain of these aspects.[55–60] However, finding the best surface topography is a great challenge, particularly due to the inability to simultaneously maximize all the necessities. Thus, optimization procedures are required that help to find the best design under the consideration of boundary conditions.[61–65] The situation becomes even more complex when further requirements such as high slip length to reduce the drag in under water flow,[66] optical properties such as transparency or anti-reflectivity,[67,68] directed wetting for droplet driven transport,[69] freezing delay for anti-icing surfaces [70] or switchability between wetting and non-wetting states [71,72] have to be fulfilled.

In this review, we focus on the progress of robust, non-wetting surfaces inspired by the cuticle of springtails (Collembola). The cuticle of these small, soil-dwelling animals exhibits water and even oil-repellent wetting characteristics in combination with a certain robustness to resist abrasion of soil particles and to survive impacting droplets of rain showers. This results from an evolutionary adaptation to maintain cutaneous respiration in temporarily flooded soil habitats. Taking these characteristics together, the collembolan cuticle addresses the list of drawbacks mentioned above and may help to overcome these limitations and to pave the way for novel promising surface modification strategies.

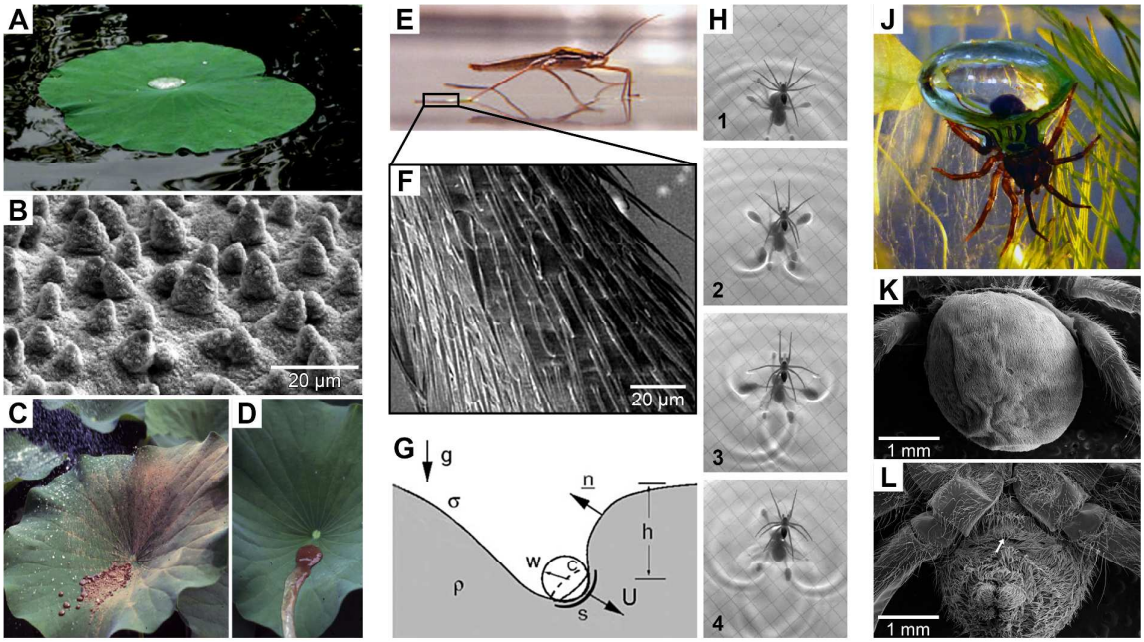

Figure 1. Examples of water-repelling natural surfaces. (A-D) Superhydrophobic lotus leaves (*Nelumbo nucifera*) exhibiting waxy, epicuticular hierarchical structures with self-cleaning properties. **(E-G)** Water strider (*Gerris*) leg featured with micro-setae providing locomotion on water surfaces. **(H)** Rowing by the fisher spider (*Dolomedes*). **(J-K)** Diving bell of the water spider (*Argyroneta aquatica*) that exhibits a hairy non-wetting mat on the abdomen. (A) reproduced from Ref. Cheng *et al.*[73]; (B-D) reprinted from Ref. Koch *et al.*[21] and (E-G) from Ref. Bush *et al.*[28], with permission from Elsevier; (H) reproduced from Ref. Hu and Bush[32], with permission from Cambridge University Press; (J) reproduced from Ref. Seymour and Hetz[40], with permission from The Company of Biologists; (K,L) reproduced from Ref. Kang *et al.*[74] under a Creative Commons Attribution 3.0. Full terms at http://creativecommons.org/licenses/by/3.0.

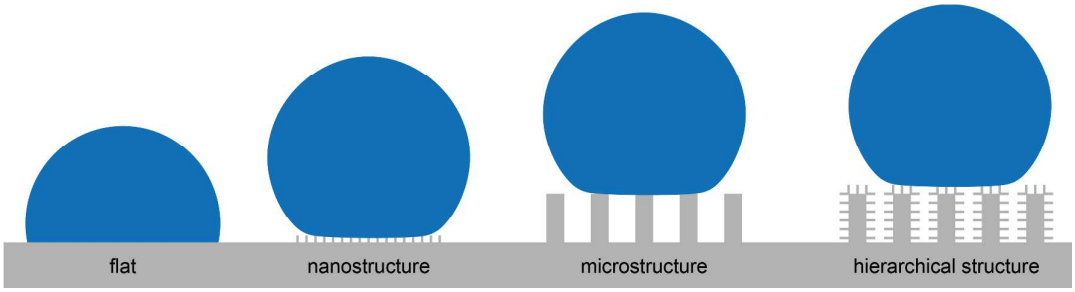

Figure 2. **Schematic illustration of four different non-wettable surfaces.** The contact area between the droplet (blue) and the surface (gray) is reduced by surface roughness (nano- and microstructure as well as the hierarchical structure) in comparison to the flat surface. All displayed rough surfaces are principally able to repel droplets. Adapted from Ref. Bhushan and Jung[47], with permission from Elsevier.

2. Wetting on solid surfaces

The wetting of solid surfaces is an important characteristic that needs to be understood and controlled, in particular, in technological processes and many areas of fundamental research.[75] As an example, one can consider an aqueous droplet originating from rain or fog: Upon contact the droplet may spread out over the entire surface or may be completely repelled. Furthermore, the droplet may slide along a certain direction across the surface or may stick to a certain region of the surface. The physicochemical origin of the individual behaviors relies on the interaction of the aqueous phase, the solid (often roughened) surface, and the surrounding media. The capillarity and wetting phenomena of such a three phase system were first reported by Young [76], Laplace, [77], and Poisson [78] in the early nineteenth century. Young, for example, qualitatively described the wetting contact angle related to the interfacial energies involved in the three-phase system, which was later proven by Gibbs [79] under thermodynamic considerations. The contact angle, which is the most widely used parameter to characterize the wetting characteristics of solid surfaces, is defined as the angle between the tangents of the liquid-vapor and the liquid-solid interface that intersect at the three-phase contact line. On ideal, smooth, inert surfaces the intrinsic contact angle, θ^{Y}, can be described by Young's equation:

$$\cos\theta^{\mathrm{Y}} = \frac{\gamma_{sv}-\gamma_{sl}}{\gamma} \quad , \tag{1}$$

where γ_{sv}, γ_{sl}, and γ are the interfacial energies between the solid-vapor, the solid-liquid, and the liquid-vapor phase boundary, respectively. By convention, there exist a transition at $\theta^{\mathrm{Y}} = 90°$ from wetting ($\theta^{\mathrm{Y}} < 90°$) to non-wetting ($\theta^{\mathrm{Y}} > 90°$) surfaces that drastically influences the behavior of a liquid. For example, capillary rise for $\theta^{\mathrm{Y}} < 90°$ or capillary depression for $\theta^{\mathrm{Y}} > 90°$ in geometrical confinements such as pores or capillary tubes can be observed. Likewise the macroscopic, apparent contact angle, which is determined by inspection of the whole droplet using contact angle goniometry, often varies from the intrinsic one on a rough surface. This was first considered by Wenzel in 1936,[80] who evolved a geometrical model based on the roughness factor, r, the ratio between the actual surface area and the projected surface area of a rough solid surface. In his model, the liquid completely wets the whole surface that is referred to as homogeneous wetting or Wenzel state. The Wenzel contact angle, θ^{W}, can be calculated as follows:[80]

$$\cos\theta^{\mathrm{W}} = r\cos\theta^{\mathrm{Y}}. \tag{2}$$

Consequently, the roughness enhances ($\theta^{\mathrm{Y}} < 90°$) or decreases ($\theta^{\mathrm{Y}} > 90°$) the wettability of a solid surface, which means the roughness amplifies the surface wettability. For intrinsically non-wettable solids, the attraction of the liquid to the solid is much lower than to wettable one. Hence, the surface tension may dominate the three-phase system, which forces the liquid to form a droplet. Thus, the liquid no longer conforms to the solid surface but rests on top of the asperities instead, while air pockets are simultaneously formed underneath the liquid.[81] This heterogeneous wetting state is referred to as Cassie or fakir state.[82] The apparent Cassie-Baxter contact angle, θ^{CB}, for a flat-topped surface can be calculated by:[83]

$$\cos\theta^{\mathrm{CB}} = r_f f_s \cos\theta^{\mathrm{Y}} + f_s - 1, \tag{3}$$

in which f_s is the fraction of the projected area of the solid surface that is wetted by the liquid, and r_f is the roughness ratio of the wetted area.

In dynamic contact angle goniometry on a rough solid surface, the moving three-phase contact line may pinned at the surface features leading to a deformation of the droplet and a variety of apparent contact angles, $\Delta\theta^{app}$, and, thus, liquid droplets are often not in thermodynamic equilibrium (i.e., the global energy minimum corresponding to Eqs. 1 to 3). They are in metastable states that can be analyzed by terms of the Gibbs energy.[84] The lowest feasible contact angle is referred to as receding contact angle, θ_r^{app}, and the highest obtained contact angle is referred to as advancing contact angle, θ_a^{app}. The difference between both angles is defined as contact angle hysteresis, $\Delta\theta^{app}$. Note that this behavior can be found also for perfectly smooth surfaces due to inhomogeneity of the surface chemistry or due to attractive forces between the liquid and the solid phase.

In summary, two models have been elaborated to evaluate the behavior of a droplet on a rough surface: In the Cassie state, liquids can be sustained at the top of asperities, and air is trapped inside the grooves of a rough surface underneath the liquid resulting in a minimal solid-liquid contact area. In the Wenzel state, liquids can penetrate grooves and wet an entire rough surface characterized by a maximal solid-liquid contact area. Calculations of the global minimum in Gibbs energy predicts which of these two states is energetically favorable for a given system, depending on the surface geometry, topography and local wettability.[83,85] Furthermore, the way (deposition, immersion, or vapor condensation) in which the liquid is brought into contact with the solid surface is important.[84] However, the Cassie state is only metastable and can be transferred to the Wenzel state by means of external energy that leads to the displacement of the entrapped air. Geometric parameters of rough surfaces have been discussed to influence the energy barrier that must be overcome for complete wetting (see section 4).

2.1. Omniphobicity

Based on intensive research on pillar structures with straight sidewalls conducted over the last decades, it was proposed that essentially low-surface-energy coatings based on fluoro- or hydrocarbons are required to achieve the Cassie state (as a pre-requisite for superhydrophobicity), i.e., an intrinsic hydrophobicity of the material coming into contact with the aqueous phase. For liquids with much lower surface tension than water, such as alkanes or polar and non-polar solvents, no material is known that is non-wettable showing intrinsic contact angles higher than 90°. Already in 1997 however, the first water and oil repellent surface, commonly referred to as an omni- or amphiphobic surface, was reported by Tsujii *et al.*.[86] The authors experimentally obtained a Cassie state of several liquids such as alkanes, esters and aromatic hydrocarbons with surface tensions ranging between 20 and 40 mN/m, although θ^{Y} on the highly fluorinated surface was below 90°. In 2000, Herminghaus suggested a theoretical strategy for maintaining the Cassie state in intrinsically wettable materials by the implementation of surface features exhibiting overhangs, which inhibit liquid penetration into the grooves of the surface via capillarity.[87] These findings clearly demonstrated that in order to obtain omniphobic surfaces the geometry, particularly the vertical structure, of the surface features plays a key role, whereas the surface chemistry has only a diminished effect. We will stress this argument in section 4, where we discuss the robustness of the Cassie state depending on the intrinsic wettability of the surface, which directly corresponds to the surface chemistry. However, the minor role of the chemistry with regard to wettability paves the way in separating intrinsic wettability from surface morphology. This point of view is contrary to the traditional approach although it has high

potential for novel routes to integrate functional groups that may help develop or optimize smart surfaces and novel applications.

Thermodynamic analysis could confirm that surface features with overhanging cross-sectional profiles can maintain a heterogeneous state even for $\theta^{Y} < 90°$.[85,88,89] In addition, several experimental studies support the geometrical concept of re-entrant structures or surface features exhibiting overhangs, and numerous rough surfaces such as porous metal surfaces,[86,90,91] certain polymers [92,93] or oxide-based [68,94] structures, fiber mats and fabrics,[95,96] pillar structures,[56,97–99] or hierarchical structures [100] could be engineered and characterized. Recent reviews focus on the design, preparation, characterization and application of omniphobic surfaces.[48,63,93,101,102]

However, omniphobicity in natural surfaces is rare, but some attention should be drawn to springtails (Collembola) (**Figure 3**). The cuticle of these animals exhibits omniphobicity that enables the formation of a stable Cassie state upon immersion into water (**Figure 3B**) and even into many low-surface-tension liquids such as alkanes or polar and non-polar solvents (**Figure 3C**).[103,104] In addition, it was found that these plastrons show a high resistance to collapse even at elevated hydrostatic pressures.[103–105] This exceptional wetting resistance is based on the hierarchically aligned micro and nanostructures of the skin surface, as detailed in section 3. Other examples in nature showing omniphobicity include *Bacillus subtilis* biofilm colonies and brochosomes covering the integuments of leafhoppers such as *Alnetoidia alneti*, *Athysanus argentarius*, and *Cicadella viridis*.[106,107] Epstein *et al*. found that the biofilm colonies and pellicles of *B. subtilis* are non-wetting even up to 80% ethanol and discussed their biocide resistance (**Figure 4A,B**).[106] Rakitov and Gorb reported that nanoscopic protein-based particles, so called brochosomes, are non-wettable for both high-surface-tension liquids and low-surface-tension liquids due to their re-entrant structure.[107] They discussed that the non-wettability of these particles protect them from contaminations or getting trapped into liquid exudates produced by leafhoppers as a consequence of their feeding on plant sap.

Recently, Wong *et al.* reported on omniphobic surfaces inspired by *Nepenthes* pitcher plants.[108] Here, the concept is different from the above discussed examples, because the wetting behavior is mainly determined by a fluorinated fluid lubricant (instead of entrapped air) that is immobilized on a micropatterned substrate. The lubricant makes the surface slippery and has the ability to recover upon damage.[109] Slippery liquid-infused surfaces (SLIPS) are, furthermore, robust against high pressures, resist bacterial biofouling[110] and ice adhesion[111] (for review see Ref. Wong *et al*.[17]).

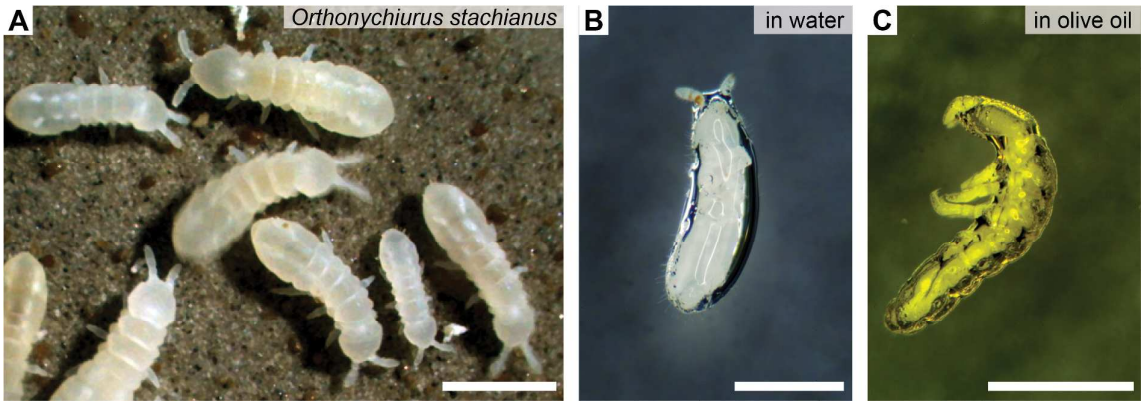

Figure 3. Omniphobicity of springtails (Collembola). (A) Springtail colony of *O. stachianus*. **(B,C)** Plastron surrounding the entire animal upon immersion into **(B)** water and **(C)** olive oil. Scale bars: 1mm. Adapted with permission from Ref. Hensel *et al*.[104], Copyright 2013 American Chemical Society.

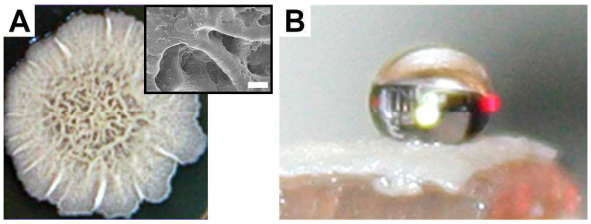

Figure 4. Omniphobicity of biofilm colonies. (A) *Bacillus subtilis* biofilm colonies. Insert shows SEM micrograph of the biofilm topography. Scale bar: 100 μm. **(B)** 50% ethanol-water solution deposited on the biofilm. Reprinted with permission from Ref. Epstein *et al*.[106]

3. Springtails and their cuticle characteristics

Recently, a conceptually novel approach to create water and oil repellent surfaces – inspired by the springtail cuticle – was developed that may provide strategies to design and fabricate more robust surfaces in comparison to lotus leaf-inspired surfaces.

Springtails (Collembola) are small (0.1-9 mm), primarily wingless, six-legged animals (hexapods) with more than 8000 species.[112–114] The name springtail is derived from a ventral, forked appendage, the furca, which enables the animals to jump and escape predators. The external and internal systematics of Collembola are still in discussion, but recent phylogenetic analyses indicated that Collembola most probably represent a sister clade to Insecta within the subphylum Hexapoda (Entognatha: Collembola).[115,116] For the first time, springtails appear in the fossil record within the early Devonian about 400 million years ago.[117–119] Today, they colonize several soil habitats, but also inhabit water surfaces of lakes, marshes or littoral zones, plants, including tree canopies, and other often extreme habitats such as deserts, caves, the Artic, and the Antarctic, where they evolved sophisticated strategies to adapt to these extreme conditions.[120–125] Thus, springtails are assumed to be the most widespread and abundant arthropods on Earth. Within the community of soil-dwelling animals, they form an integral part of the food web and decompose organic materials into inorganic forms by grazing microorganisms such as bacteria, fungi, or algae.[126,127]

3.1. Wetting characteristics

Differing from insects, which breathe using tubes called trachea, most springtail species take up oxygen by cutaneous respiration (except *Symphypleona,* which developed simple tracheal systems).[128,129] This means that the gas exchange, which is driven by diffusion, occurs through the cuticle over the entire body surface. To maintain the cutaneous respiration, the cuticle surface needs to be kept dry, clean, and has to be mechanically robust; otherwise the gas transfer rate would be substantially affected leading ultimately to suffocation.[103,130] To avoid wetting, most springtails exhibit a superhydrophobic surface (**Figure 5**) maintaining a stable Cassie state upon contact with water. This leads to the formation of a protective air layer upon immersion, the plastron, forming a gas reservoir that enables regular gaseous exchange under water (**Figure 3B,C**).[34,103,131,132] Recently, Gundersen *et al*. reported that the littoral Collembola *Cryptopygus clavatus* lives submerged in summer and respires through direct gaseous exchange with water lacking any support of a plastron. This strategy is also found in other arthropods, eggs and larvae of which in particular seem to benefit from circumventing the buoyant forces of a plastron that would lift the animals to the surface.[133] Interestingly, *C. clavatus* is able to adapt to winter conditions, when it lives on dry land, by changing the wetting characteristics to a pronounced repellent cuticle surface that subsequently enables plastron formation upon immersion.

The superhydrophobicity of the collembolan cuticle leads to a passive drift when floating on a water surface or displacement by wind. This passive drift is assumed to distribute springtails along the water flow or on water surfaces and represents a possibility for a variety of species to disperse over long distances and even initiate the colonization of new islands.[134,135] Some species that commonly live in aquatic habitats such as *Anurida maritima* or *Podura aquatica* exhibit the capability not only to float passively, but also to walk actively on water surfaces by meniscus climbing or leaping using the furca and the water surface as a drop zone

(**Figure 6**).[136,137] It was found, therefore, that the cuticle is not uniform in its wetting properties.[138,139] The cuticle covering the ventral tube and the claws on the tips of the limbs are examples of readily wettable body regions and both support the animal's locomotion.[27,28,138]

The repellence of aqueous media evolved by the collembolan cuticle has been known for more than a century.[140,141] However, the remarkable wetting resistance of the skin surfaces even against wetting by a variety of low-surface-tension liquids such as non-polar alkanes or polar solvents (e.g., ethyl alcohol or acetone) was only recently demonstrated by immersion test and visibly proven by the formation of plastrons (**Figure 5C**).[103] It is presumed that these findings reflect the adaptation to habitats where water is contaminated with surface-active substances originating from decaying organic matter.[142]

3.2. Structure of the collembolan cuticle

In the 1960s and 1970s, optical and electron microscopy revealed the hierarchically arranged and highly textured springtail cuticle.[143–145] The unique ornamentation typically consists of nanoscaled primary granules (minor tubercles) and interconnecting ridges; together forming nanocavities that are arranged in a rhombic or hexagonal comb-like pattern, which covers the entire body (**Figure 7**). Several studies showed that the nanoscopic comb structures are rather similar, reflected in the diameter of the cavities between 0.3 and 1 µm.[130,131] In addition, the comb structure exhibits characteristic overhangs in a cross-sectional view.[103,146] At the microscopic scale, some species that live primarily in soil possess papillose secondary granules (major tubercles) that are completely decorated by the comb structure. It is presumed that this undulating landscape mechanically protects the integrity of the nanostructures by reducing the contact area between cuticle surface and the surrounding soil particles.[130,145] Thin bristles (setae) or scales form the tertiary structure complete the hierarchical assembly of the collembolan cuticle. Their degree of coverage also depends on the habitat and is quite sparse for soil-dwelling springtails.[147,148] In summary, the occurrence of the secondary granules and the bristles or scales as tertiary structures show a high diversity and clear ecological and taxonomic dependency, thus contrasting the uniformity of the nanoscopic comb structure.[112,130,131,144,148,149]

3.3. Chemistry of the collembolan cuticle

In the normal direction to the surface, the collembolan cuticle exhibits a layered structure commonly observed for arthropods.[143,147,150,151] Recently, a chemical analysis of *Tetrodontophora bielanensis* cuticles collected after molting supported these observations, but furthermore revealed the chemical components of the vertically layered structure, namely (from the inside to the outside), a chitin-rich lamellar procuticle covered by a protein-rich epicuticle (i.e., the comb forming structure) and an outermost lipid-rich layer forming an envelope a few nm in thickness (**Figure 8**).[152] The wax-like surface coating had already been indirectly proven about 50 years ago by Noble-Nesbitt [138] using chloroform extraction and by Ghiradella & Radigan [147] using lanthanum staining. Both studies concluded that this layer helps to ensure hydrophobicity under wet conditions and to prevent desiccation under arid conditions. Although such a thin lipid layer would enable gaseous exchange, it hardly protects against transpiration and desiccation.[149] Recently, a study combining time of flight secondary ion mass spectrometry (TOF-SIMS), thin layer chromatography (TLC) and gas chromatography mass spectrometry (GC-MS) revealed a mixture of lipids such as fatty acids, steroids and terpenes.[152] This composition may vary between different species and also

seasonally, enabling temporary adaption to varying habitat conditions, as recently supposed for *C. clavatus*.[133] In addition, fatty acids and terpenes are suggested to afford the non-fouling characteristics of the cuticle surface due to their intrinsic antibacterial effect.[153–155] In a first qualitative approach, *T. bielanensis* was exposed to *Escherichia coli*, *Staphylococcus aureus* and *Candida albicans* representing Gram-positive bacteria, Gram-negative bacteria, and fungi, respectively, for four days each under standard culture conditions without observing any significant deposition.[103] Likewise, terpenes are known as defence substances of plants and insects and may therefore serve as a protection of the cuticular surface against microbial attack.[156] Furthermore, several studies prove that the lipid layer is not covalently bound to the epicuticule as it could be extracted by solvents or mechanically removed by shaking animals in dust particles.[138,152,157] Lipids rather continuously migrate towards the surface, where they permanently recover the coating. Likewise, it is conceivable that the lipid film forms a continuously reproduced sacrificial layer to avoid microbial colonization; a hypothesis, however, that needs further investigation. A complete recovery of the whole cuticle occurs during moulting as a result of growth.[158,159]

The recent chemical analysis of Nickerl *et al.* further revealed that the primary granules and interconnecting ridges, together forming the epicuticule or cuticulin layer [143,152,160], are mainly composed of proteins with high amounts of glycine, tyrosine and serine. The composition of the amino acids, which was analyzed by high performance liquid chromatography (HPLC), resembled that of known structural proteins such as fibroin, collagen or resilin [161–163] that often combine stiffness and toughness.[164] The durability of these epicuticular structures was further demonstrated by sand blast experiments and showed a much higher resistance compared to the wax crystals of superhydrophobic plant surfaces.[103] A rational conclusion is that the durability of patterned collembolan cuticle in withstanding wear and friction in soil habitats results from protein structures. However, a detailed mechanical analysis of the comb structure and, in particular, the role of the secondary granules, which seems to be essential to avoid damage by soil particles, is still lacking.

3.4. Replication of epicuticular surface morphology

In order to distinguish between effects of surface chemistry in comparison to surface morphology and, furthermore, to resolve the impact of the individual structural elements on water and oil repellency of the collembolan cuticle, Hensel *et al.* developed an adaptive replication process that is illustrated in **Figure 9A**.[105] Perfluoropolyether dimethacrylate (PFPEdma) was used as elastomeric mold material that primarily ensures high accuracy of the finally replicated polymer structures.[165] Hensel *et al.* produced polymer skin replicas of similar chemical bulk composition, but with distinctive surface morphologies regarding the presence of the nanoscopic granules and surface chemistries. The contact angle data (**Figure 9B**) showed a clear correlation with the particular surface morphologies: Polymer replica surfaces containing nanoscopic primary granules revealed contact angles considerably higher than 90°, with values up to 150° for water and hexadecane (as an oily liquid), reflecting an omniphobic wetting performance irrespective of the polymer surface chemistry. In contrast, the polymer replicas without the nanoscopic primary granules of the springtail skin were completely soaked by both test liquids resulting in macroscopic contact angles close to 0°. Teflon-AF-coating of the latter replicas afforded water repellence but were completely soaked by hexadecane. These results provided new insights into the structural and chemical origin of the wetting resistance of springtail skins. Contact angle goniometry of a series of imprinted polymer replicas clearly identified the nanoscopic primary granules of

the cuticle to be essential in liquid repellence. This study could prove the suggestions of Helbig *et al.* that the overhangs of the nanoscopic granules visible in cross sections provoke an energy barrier to be overcome by the advancing liquid phase, even one with a low surface tension.[103]

A

species	θ_a^{app}	θ_r^{app}	$\Delta\theta^{app}$	SG
Hypogastura viatica	$167.9\pm1.5^\circ$	$163.2\pm1.6^\circ$	$4.7\pm2.2^\circ$	yes
Isotomurus prasis	$168.2\pm3.3^\circ$	$164.1\pm3.7^\circ$	$4.1\pm4.9^\circ$	no
Onychiurus sp.	$170.2\pm2.4^\circ$	$166.2\pm2.9^\circ$	$4.0\pm3.8^\circ$	yes
Folsomia quadrioculata	$170.5\pm2.6^\circ$	$166.5\pm2.0^\circ$	$4.5\pm2.6^\circ$	no
Anurophorus septentrionalis	$168.3\pm2.3^\circ$	$164.8\pm2.4^\circ$	$3.5\pm3.4^\circ$	no
Desoria olivacea	$164.4\pm3.7^\circ$	$162.5\pm2.1^\circ$	$1.9\pm4.8^\circ$	no
Archisotoma besselsi	$169.6\pm2.2^\circ$	$164.5\pm3.1^\circ$	$5.0\pm3.8^\circ$	yes*
Cryptopygus clavatus	$140.6\pm3.1^\circ$	$118.4\pm10.9^\circ$	$22.3\pm11.4^\circ$	no
Orchesella flavescens	$150.2\pm6.0^\circ$	$152.9\pm4.4^\circ$	$-2.7\pm7.5^\circ$	no
Anurophorus laricis	$157.4\pm2.5^\circ$	$161.2\pm8.3^\circ$	$-3.8\pm8.7^\circ$	no
Isotoma anglicana	$154.3\pm4.0^\circ$	$158.6\pm1.9^\circ$	$-4.3\pm4.5^\circ$	no
Xenylla maritima	$156.5\pm9.8^\circ$	$132.4\pm11.9^\circ$	$24.1\pm15.4^\circ$	no

B

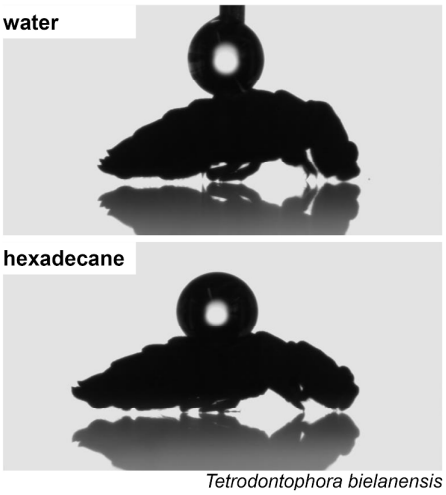

Tetrodontophora bielanensis

C

polar liquids	skin wetting	γ (mN/m)	nonpolar liquids	skin wetting	γ (mN/m)
ethanol	no	22.1	hexane	yes	18.0
methanol	no	22.2	decane	yes	23.5
acetone	no	23.4	cyclohexane	yes	24.7
butanone	no	23.9	dodecane	yes	24.9
1-pentanol	no	25.3	tridecane	no	25.6
2-heptanone	no	26.1	chloroform	no	26.9
Water	no	72.3	hexadecane	no	27.1

Figure 5. Wetting characteristics of the collembolan cuticle. (A) Results of dynamic contact angle goniometry for several species with absence and presence of secondary granules (SG): advancing (θ_a^{app}) and receding (θ_r^{app}) contact angles and determined contact angle hysteresis θ^{app}. **(B)** Droplets of polar high surface tension liquid (water) and nonpolar low surface tension liquid (hexadecane) deposited dorsally on collembolan cuticle. **(C)** Results of immersion tests of three different species in polar and non-polar liquids. (A) reproduced from Ref. Gundersen *et al*.[131] and (C) reproduced from Helbig *et al.*[103] both under a Creative Commons Attribution 4.0. Full terms at http://www.creativecommons.org/licenses/by/4.0/.

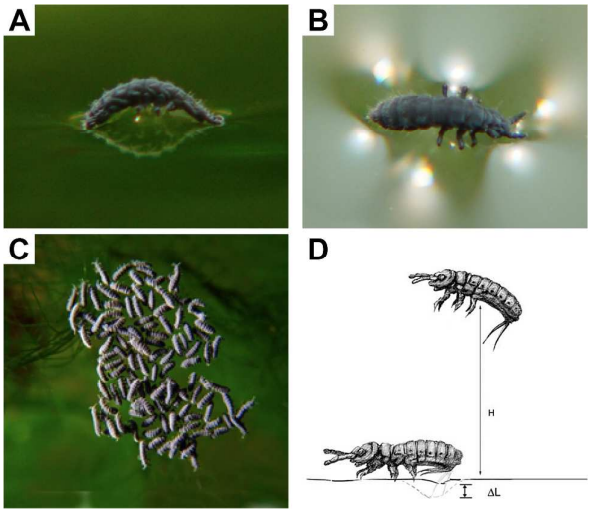

Figure 6. Active locomotion on water surfaces: (A,B) Meniscus-climbing as a strategy for **(C)** colony formation of *Anurida maritime* and **(D)** leaping by *Podura aquatica*. (A-C) reprinted from Ref. Bush *et al*.[28], with permission from Elsevier; (D) reprinted from Ref. Hu *et al*. [137], with permission from Springer.

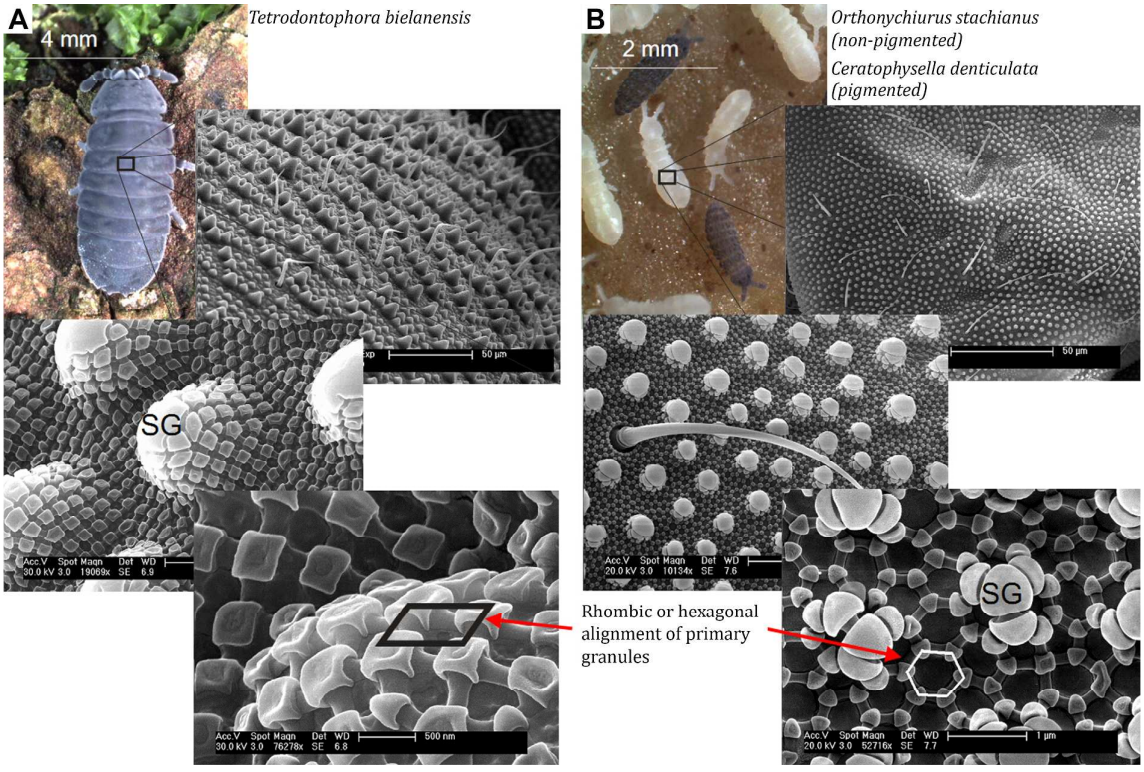

Figure 7. Hierarchically assembled collembolan cuticle that combines bristles, papillose secondary granules (SG) and a unique nanoscopic comb pattern: (A) The rhombic comb pattern of Tetrodontophora bielanensis or **(B)** the hexagonal comb pattern of Orthonychiurus stachianus. Reproduced from Helbig *et al.*[103] under a Creative Commons Attribution 4.0. Full terms at http://www.creativecommons.org/licenses/by/4.0/.

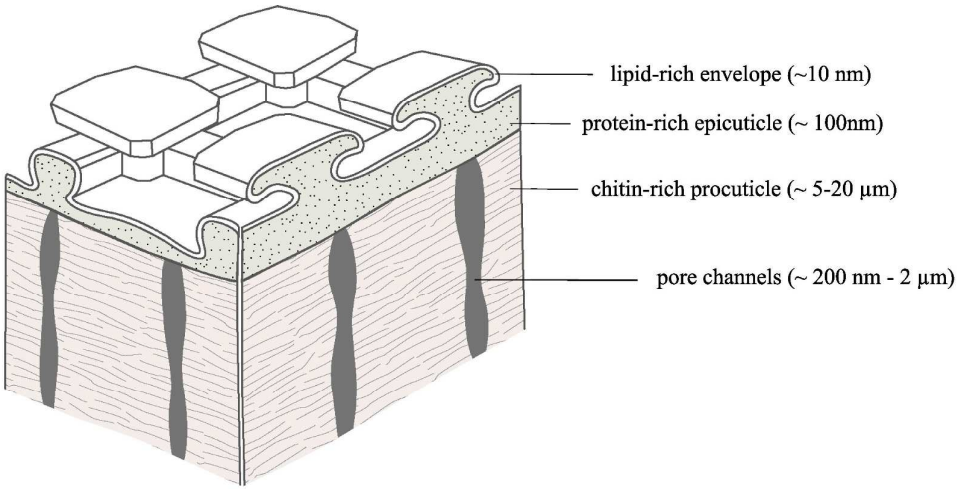

Figure 8. Chemical model of the multilayered collembolan cuticle of *T. bielanensis*. Reprinted from Ref. Nickerl et al.[152], with permission from The Royal Society.

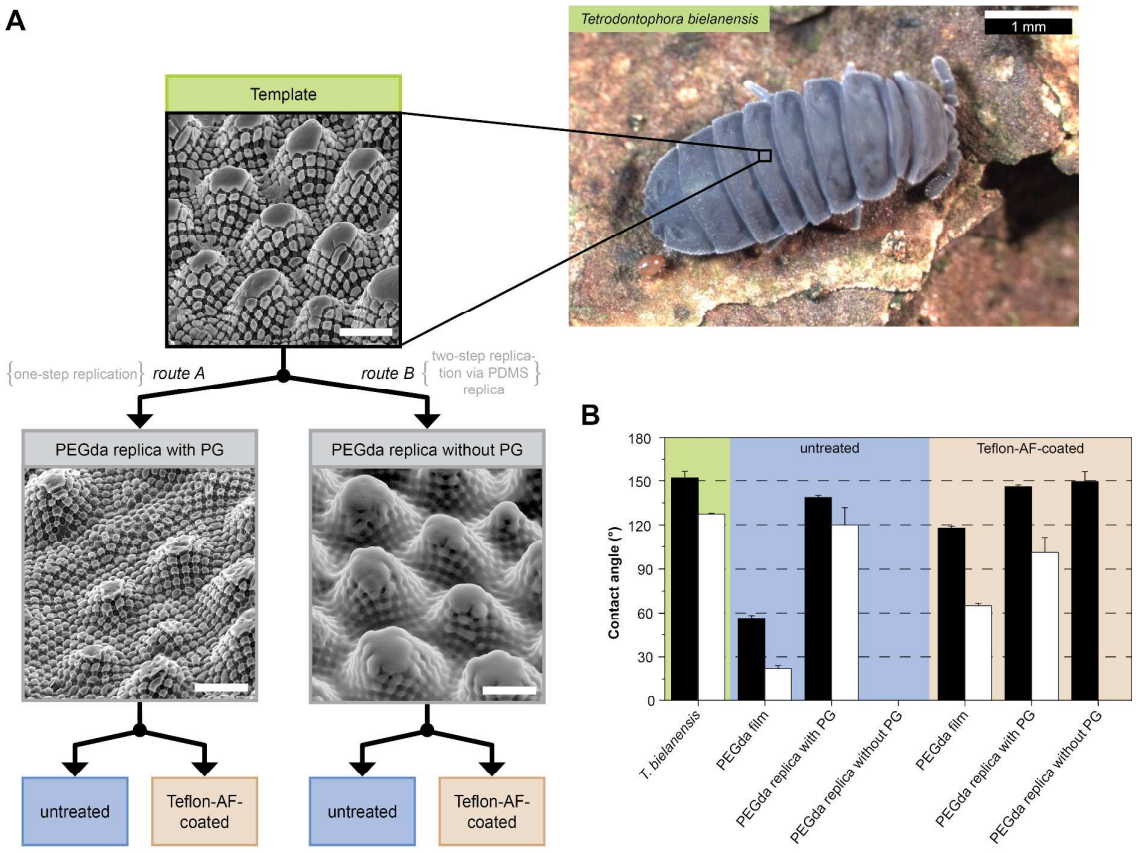

Figure 9. Cuticle replication process and the contact angle measurements. (A) Schematic illustration of the sample preparation via replication of *T. bielanensis* in which two routes are feasible albeit distinctive regarding the absence or presence of nanoscopic morphology (PG = primary granules) **(B)** Results of the static contact angles using droplets of water (black bars) and hexadecane (white bars). Adapted from Ref. Hensel *et al.*[105] under a

4. Robustness of liquid-repelling surfaces

In view of the numerous applications and products relying on liquid-repelling surfaces, which are essentially depending on the persistence of the Cassie state, a detailed understanding of the durability of those nano- and micropatterned surface is crucial. The durability critically depends on the robustness that includes both the resistance against complete wetting and the mechanical stability of the surface features. Hence, when designing omniphobic surfaces these aspects must be taken into account as much as the ability to repel various liquids itself. To identify the best shape fulfilling all these requirements, optimization procedures are inevitably needed resulting in merit functions or design maps.[64] For example, Cavalli *et al*. proposed a numerically based procedure to adjust the contact area between the top of the surface features and the applied liquid, i.e., area wetted by the liquid, by taking high apparent contact angles and a high pressure resistance against depinning of the three-phase contact line into account (see below).[65] Interestingly, they found that surface features showing branched interfacial areas perform best and matching the shape of many naturally assembled wax crystals on superhydrophobic leaves of plants. In addition, the authors implemented a filter into their numerical model to obtain only geometries that are feasible to fabricate using optical lithography. Note that further requirements such as optical properties, mechanical stability, resistance against biofouling, and so on need to be considered in certain applications. Those multi-functional surfaces then probably result in completely different shapes for optimized surface features and reflect a balanced compromise to keep all required functions. In the following two sections, we will summarize the main concepts to obtain durable, liquid-repelling surfaces by focusing on the most robust designs protecting surfaces against complete wetting and mechanical loads.

4.1. Cassie-Wenzel wetting transition

By definition, the wetting transition is an abrupt change in the wetting properties of a droplet on flat or rough solid surfaces or in binary liquid mixtures either spontaneously or induced by external stimuli.[166,167] Surface roughness has been shown to affect macroscopic surface wetting properties significantly because two different wetting regimes, namely the Cassie and the Wenzel state can coexist, while the Cassie state is metastable and can be transferred to the Wenzel state.[82,168] To induce the wetting transition from the Cassie to the Wenzel state, an energetic barrier has to be overcome (**Figure 10**).[169–171] The barrier can be achieved by the intrinsic energy of the droplets itself or by external triggers. In nature, the liquid-repellent cuticular surfaces of plants and animals mainly have to resist the kinetic energy of impacting rain droplets that exhibit an inner hydrostatic pressure in the range from 10^4 to 10^5 Pa or droplet formation from condensation at high relative humidity.[172–175] Furthermore, droplets that are not repelled, but stuck onto the surface, continuously enhance their inner pressure due to evaporation accompanied by shrinkage of the droplet size.[176] On the other hand, the transition can be externally enforced by the compression of the liquid in which the hydrostatic pressure is elevated, for instance, with increasing depth upon complete immersion.[103,105]

In determining the wetting transition barrier, two complementary concepts have been developed.[167,177] In the energetic approach, the Gibbs energy curve for a droplet on a real surface is taken into account, where it was shown that the Wenzel state is energetically favorable in comparison to the Cassie state (**Figure 11**). This approach allows calculating the energetic barrier to overcome this transition, however, numerical simulations are often required when the surface features exhibit a complex shape.[178–180] The concept of critical

pressure is based on Laplace's law that takes the pressure difference, Δp, across a curved fluid interface into account:

$$\Delta p = 2\gamma\kappa, \tag{4}$$

where κ is the fluid interface curvature. Thus, an elevated hydrostatic pressure has an influence on the curvature of a fluid interface that, for example, leads to a local sagging of the interface between adjacent surface features. In turn, a sagging fluid front can induce a wetting transition by two different scenarios: The sagging results in a contact of the fluid front with the bottom of the substrate while the position of the three-phase contact line remains unchanged (**Figure 12A**). Alternatively, the sagging enforces the propagation of the fluid front along the sidewall upon depinning of the three-phase contact line (**Figure 12B**). The two different transition scenarios can be controlled, for example, by the height of the surface features.[181] The depinning scenario, which is also referred to as the canthotaxis effect, can be theoretically described by the Gibb's criterion that expresses a continuous variation of the actual contact angle, θ^*, at a certain position of the three-phase contact line within the range of:

$$\theta^{\mathrm{Y}} \leq \theta^* \leq \theta^{\mathrm{Y}} + (\pi + \Psi), \tag{5}$$

where Ψ represents the geometrical edge angle. Note that for an advancing liquid front, the Young's contact angle in Eq. 5 should be replaced by the advancing contact angle, θ_a. The critical pressure difference, Δp_{break}, that induces the breakthrough scenario can then be determined using Eq. 1,4, and 5:

$$\Delta p_{break} = \frac{2\gamma \sin(\theta^{\mathrm{Y}} + \Psi)}{x}, \tag{6}$$

where x is the distance between the three-phase contact line and the symmetry center of two adjacent asperities with a similar shape(**Figure 13**). Thus, the breakthrough scenario induced by depinning (**Figure 13B**) depends on the surface tension of the applied liquid, the air pressure inside the cavity, the wettability of the material, and topographical parameters of the surface such as the geometrical edge angle, and the distance between adjacent asperities. On closer inspection, Eq. 6 includes the geometrical concept of overhanging structures, i.e., $\Psi > -\frac{\pi}{2}$. Thus, overhangs are required to establish a pressure barrier when the intrinsic contact angle is lower than 90°, i.e., common for low-surface-tension liquids even on solid substrates with low surface energy or for water on hydrophilic materials.[56,98] It was found that Eq. 6 can be further reduced to:[104]

$$\Delta p_{break} = \frac{2\gamma}{x}, \text{ when } \theta^{\mathrm{Y}} > \frac{\pi}{2} - \Psi. \tag{7}$$

Here, the critical pressure difference only depends on the surface tension of the applied liquid and the distance between adjacent asperities and, hence, is irrespective of the intrinsic wettability of the material (**Figure 13C**). In general, the geometrical edge angle may vary along the sidewall of the asperity, but is then represented by the slope, which is the arctangent of the first derivative of a known sidewall function ($\Psi \coloneqq \tan^{-1} f'(x)$). This relationship also allows estimating the breakthrough pressure for more complex geometries, such as the characteristic mushroom-shaped cross-sections of the primary granules found on springtails (**Figure 14A**).[104,146] Inspired by these surfaces, serif T structures exhibiting $\Psi = \frac{\pi}{2}$ were introduced that fulfill the condition of Eq. 7 even for completely wettable surfaces

where $\theta^{Y} \approx 0°$. Recently, Liu and Kim could experimentally prove this serif T structure concept and reported on the repellence of alkanes and even fluorinated hydrocarbons with surface tensions down to 10 mN/m on non-treated silicon oxide surfaces patterned that way (**Figure 14B**).[182] Conclusively, the springtail-inspired abstraction of a mushroom-shaped profile into serif T structures revealed a pressure barrier irrespective of the surface chemistry, which may pave the way for a free choice of surface modifications without affecting the wetting resistance. However, the proposed concept is valid only for “ideal” liquids on “ideal” substrates and does not cover liquid penetration into the cavities by swelling, intercalating, or creeping of the liquid with the solid material.[183] Furthermore, liquids containing surfactants, proteins, sugars or other organic and inorganic compounds may behave in a different manner due to adsorption processes or chemical reactions at the three-phase contact line that may vary the nature of the surface.[184,185]

To observe the Cassie-Wenzel wetting transition experimentally, various approaches have recently been developed. In particular, methods allowing for *in situ* observation of the wetting transition by interference microscopy, laser scanning confocal microscopy, synchrotron X-ray radiography and high-frequency acoustic methods were used to access its dynamics.[146,176,186–192] These methods permit the observation of interface deformations and propagation of the liquid front (**Figure 15**). The studies revealed that the transition typically consists of the impalement, i.e., the propagation of the three-phase contact line along the sidewall of the surface features and the contact of the sagging fluid front with the bottom of the substrate. Papadopoulos *et al*. found that, in their experiments, the time for the impalement corresponded to a continuously increasing hydrostatic pressure related to the evaporation rate of the deposited droplet. On the other hand, the fluid front spontaneously wetted the whole substrate within less than a second when touching the bottom of the substrate(**Figure 15A,B**).[176] Hensel *et al*. found that the impalement can be slowed down by inner constrictions inside the cavities, such as overhangs, and demonstrated that the transition barrier can be tuned by varying the sidewall profiles.[146] Lv *et al*. showed that impurities or non-regular shaped surface features can induce an asymmetrical propagation, which reduces the transition barrier (**Figure 15C**).[193]

Natural liquid-repelling surfaces are typically hierarchically organized, i.e., a nanoscopic structure overlaying a microstructure (**Figure 7**). When the microstructure exhibits a sinusoidal or box-shaped profile, the distance between adjacent nanostructures is much smaller than the distance between adjacent microstructures (**Figure 16**). Thus, the pressure resistance for penetrating the microstructures is smaller than for the nanostructures (*cf.* Eq. 6). Hensel *et al*. demonstrated that the liquid front penetrated the microscopic groove between adjacent, nanoscopic patterned surface features without soaking the nanocavities between adjacent nanostructures (**Figure 16A**).[105] The propagation of the liquid front occurred in discrete slip-stick steps that result from pinning and sag-transition phenomena. Several experimental studies found a similar characteristic. Interestingly, the first transition step is reversible, which induces the propagation of the fluid front into the microscopic grooves while air remained trapped inside the nanocavities, (**Figure 16B**).[105,194]

The dynamics of the wetting transition are still not completely understood: a critical dependence on the shape, material and arrangement of the surface features exists. In addition, the rate of increasing the hydrostatic pressure depends on the experimental setup and varies between very low rates when driven by evaporation of a sessile droplet (typical rate is in the range of Pa/s), and very high rates when falling droplets impact the surface (here the pressure increases to its maximum value within milliseconds). Moreover,

Bormashenko *et al*. reported that not only vertical but also lateral depinning of the three-phase contact line can induce a wetting transition.[195] Semprebon *et al*. demonstrated that the lateral expansion of the liquid front across the surface upon touching the bottom of the substrate strongly depends on the pillar geometries and density.[196] Butt *et al*. further introduced a transition scenario based on material transport instead of capillarity effects. Here, volatile liquids fill up the grooves of the rough substrate through continuous evaporation and condensation processes, particularly when the vapor cannot equilibrate with the surroundings, such as, upon complete immersion.[62,197]

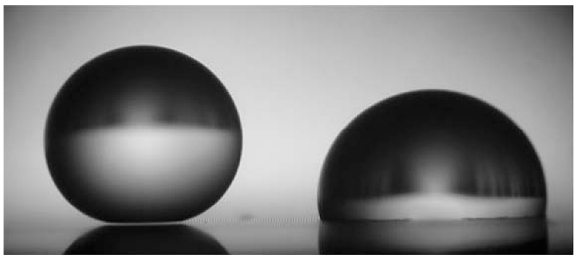

Figure 10. Millimetric water droplets deposited on a superhydrophobic substrate. The light passes below the left droplet indicating the Cassie state, while the right droplet after transition wets the surface in the Wenzel state. Reproduced from Ref. Callies and Quéré[198].

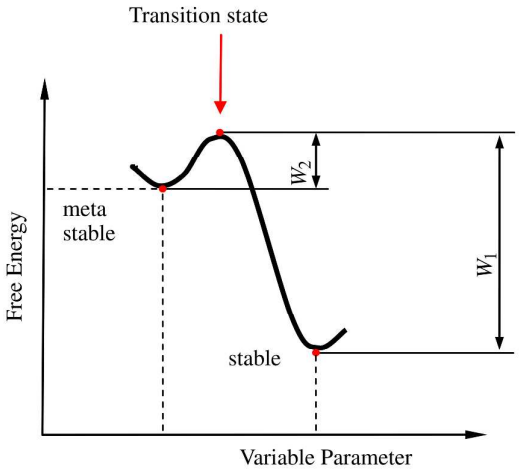

Figure 11. Schematic representation of the Gibb's energy curve for a sessile droplet on a micropatterned surface. The global energy minimum corresponds to the stable Wenzel state while the local minimum corresponds to the metastable Cassie state. W_1 and W_2 are the energetic barriers for Wenzel-to-Cassie and Cassie-to-Wenzel transition, respectively. Reprinted from Ref. Bormashenko[171], with permission from Elsevier;

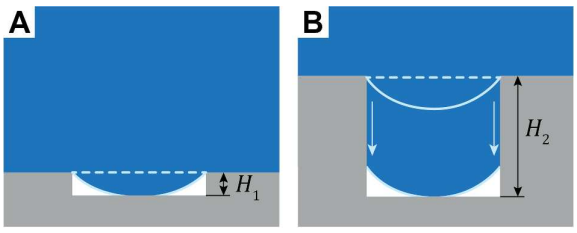

Figure 12. Enforced transition mechanism from Cassie to Wenzel state that critically depend on the height, H, of the surface features. **(A)** The sagged fluid interface touches the bottom of the substrate. **(B)** The three-phase contact line advances along the cavity sidewalls upon depinning.

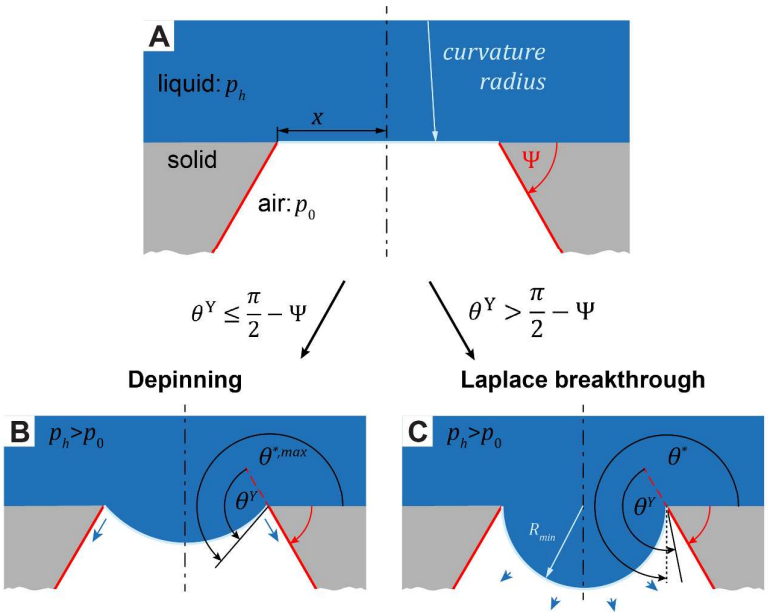

Figure 13. Illustration of two distinctive pressure-induced wetting transition phenomena that can occur on overhanging structures depending on the relationship of intrinsic contact angle, θ^Y, and the geometrical edge angle, Ψ. (A) Liquid phase sustained atop a circular cavity with the radius, x. In both phenomena considered, the liquid-air interface sags into the cavity due to continuously increasing hydrostatic pressure, p_h, whereas the air pressure, p_0, is kept constant. **(B)** Depinning of the three-phase contact line when the actual contact angle, θ^*, of the sagging liquid-air interface becomes $\theta^Y + (\pi + \Psi)$ (*cf.* **Eq. 5**). **(C)** The critical pressure difference in the Laplace breakthrough phenomenon is achieved when the sagging liquid-air interface forms a semi-circular profile that corresponds to the minimal curvature radius, R_{min}, which corresponds to the maximal Laplace pressure across the interface. Adapted with permission from Ref. Hensel *et al.*[104], Copyright 2013, American Chemical Society.

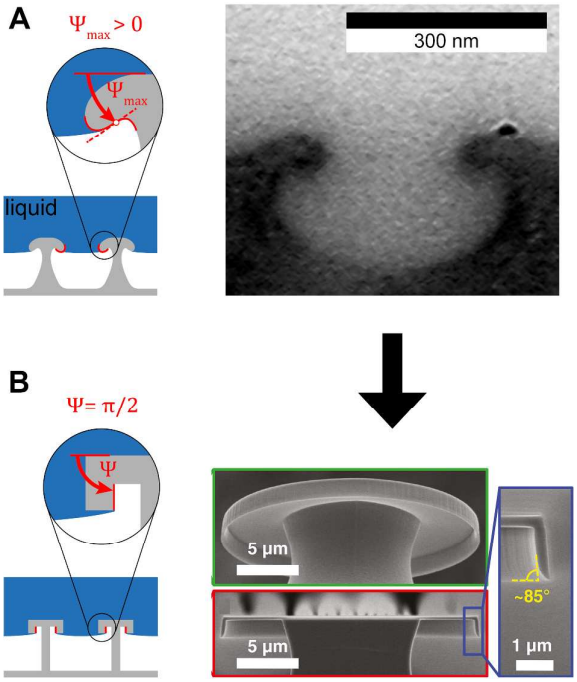

Figure 14. Springtail-inspired geometrical models for serif T structures. (A) Model and micrograph of cross-section through the collembolan cuticle of *O. stachianus*. **(B)** Model and micrographs of fabricated surfaces. Adapted with permission from Ref. Hensel *et al.*[104], Copyright 2013, American Chemical Society. Right-hand part of (B) reprinted with permission from Ref. Liu and Kim[182], with permission from AAAS.

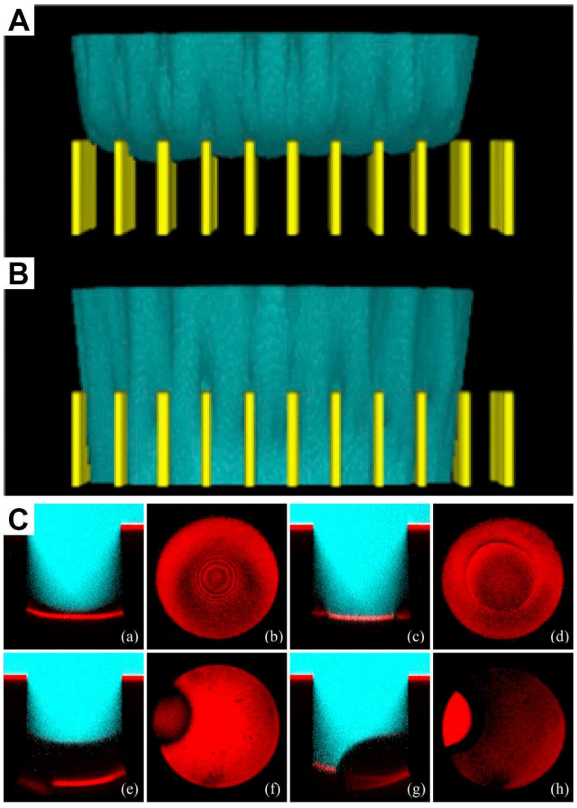

Figure 15. *In situ* observation of the Cassie-Wenzel transition using laser scanning confocal microscopy. (A) Three-dimensional image of a fluorescently labeled water drop on an array of SU-8 pillars **(B)** The same droplet after the collapse of the Cassie state. **(C)** Symmetric (a−d) and asymmetric (e−h) collapse shown in side-view line scans and corresponding top views. (A,B) reprinted with permission from Ref. Papadopoulos *et al.*[176]. (C) reprinted with permission from Ref. Lv *et al.*[193], Copyright (2014) American Chemical Society.

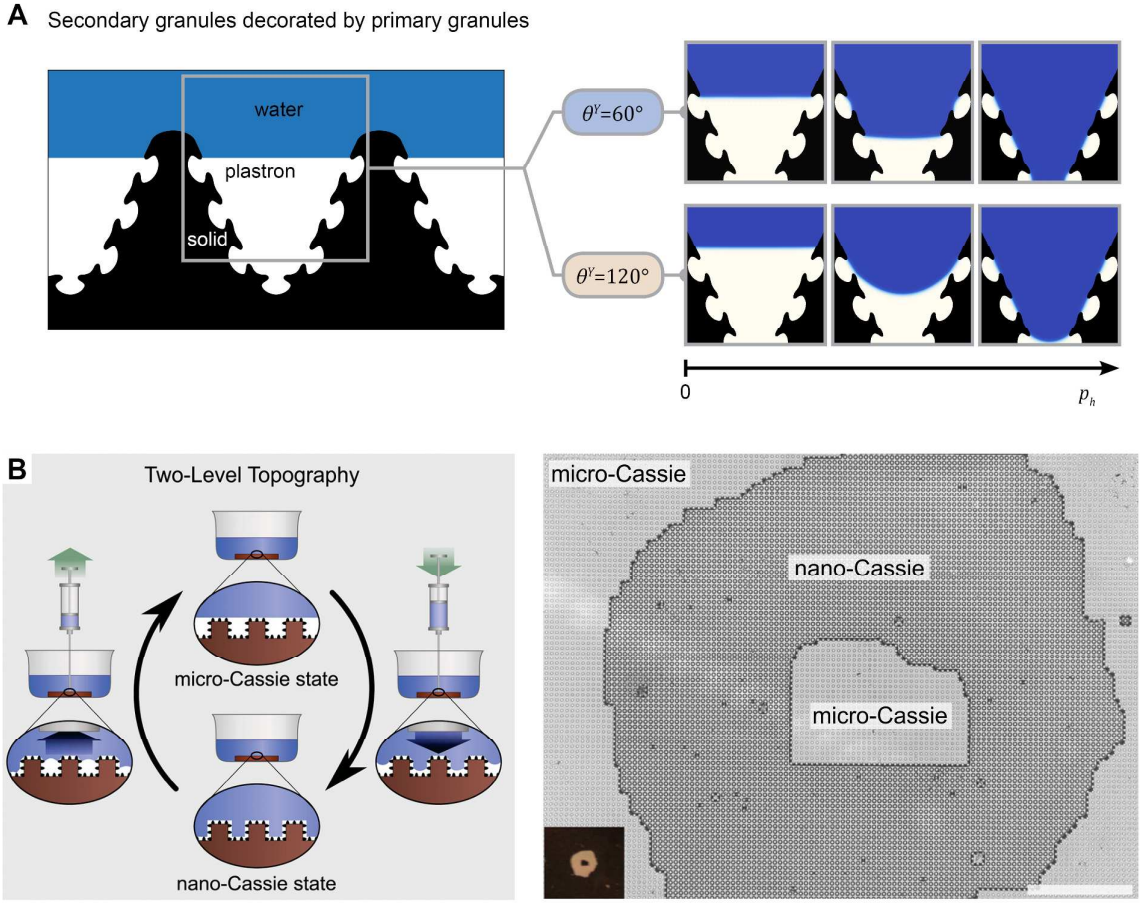

Figure 16. Cassie-Wenzel transition on hierarchically assembled surfaces. (A) Numerical finite element method simulations showing the dynamics of the Cassie-Wenzel transition. On the left, a schematic representation of a sectional view of a hierarchically assembled surface, inspired by springtails. On the right, numerical results are presented by snap shots from left to right that display the advancing liquid front (blue) displacing the plastron (white) inside certain complex shaped solid phase fields (black). Both hydrophilic and hydrophobic surfaces were considered. **(B)** Wetting states and transitions on surfaces with two-level topography. Both the micro-Cassie and the nano-Cassie state can be visualized by optical microscopy upon complete immersion of the surface. (A) adapted from Ref. Hensel *et al.*[105] under a Creative Commons Attribution 4.0. Full terms at http://www.creativecommons.org/licenses/by/4.0/. (B) reprinted with permission from Ref. Verho *et al.*[194]

4.2. Mechanical robustness

Mechanical robustness still remains a major challenge in fabricating liquid-repellent surfaces. Often the repellence vanishes after a certain time period due to the inherent fragility of the nano and microstructures. In particular, the breakage of the surface features from the substrates under shear loads or a continuous degradation of the surface features due to wear results in a different surface topography that may not uphold the original wetting characteristics. In addition, the removal of surface coatings, induced by wear or exposure to corrosive agents, may lead to a failure in repellence. To obtain omniphobic surfaces, pillar-based surface features exhibiting mushroom-shaped cross-sections were recently introduced.[97] Such structures intrinsically possess a predetermined breaking point at the tapered, overhanging part of the pillar that further decreases the shear resistance and, therefore, may dramatically shorten the life time of those surfaces (**Figure 17**).

Different approaches have been elaborated to improve the durability of liquid-repellent surfaces in general. Obviously, harder materials such as metals or ceramics might replace soft materials such as polymers. Due to the greater hardness, structures could exhibit a better resistance against wearing; however, the shear resistance may remain unchanged or even worse than for flexible soft materials due to the loss of compliance. Very recently, Elliot *et al.* proposed an attractive approach dealing with composite materials.[199] They assumed that a soft polymer shell coating covering the inner inorganic phase could enhance the flexibility of the nanostructure and afford better mechanical stability. Besides the choice of materials, the shape of the pillar structures can be tuned. A reduced height, for instance, decreases the bending momentum under shear stress. However, the predetermined breaking point of omniphobic surfaces due to the overhang usually cannot be suppressed.[61] To overcome this limitation mechanically, self-supporting networks such as interpenetrating fibrous structures,[200] close-packed assemblies of colloidal particles,[68] woven fabrics[95] or even the comb structure found on springtails (**Figure 7**), in which adjacent surface features are interconnected, appear promising due to a better shear load dissipation than that of individual pillars. Hensel *et al.* proved the concept by fabricating polymer membranes that resisted higher shear loads when manufactured as pillar structures.[197] The proposed concept may have a negative impact on the capability to repel liquids due to a proportionally larger area that is wetted by the liquid than on pillar surfaces; however, a hierarchical assembly of the self-supporting networks onto undulated surfaces might have the potential to overcome this drawback.

A completely different approach to resisting wear is the permanent renewal of the surface including structures and coatings. Nature accomplishes this through continuous growth and several self-healing capabilities. For example, most plants segregate lipid compounds such as waxes by diffusion to the cuticular surfaces where they crystallize and replace damaged surface features.[201] In contrast, hemimetabolic insects renew the whole cuticle by molting several times during their life cycle. In artificial systems, the main concept of self-healing, liquid-repellent surfaces are based on the encapsulation of hydrophobic agents into pores of the surfaces. Upon damage, these agents quickly migrate to the damaged surface and recover it repellence.[202] Jin *et al*. could transfer this principle to omniphobic surfaces made of porous silica aerogels. Silica nanoparticles loaded with silanols could replenished the new surface upon local damage of the aerogel while the overhanging geometry was preserved throughout the whole aerogel coating.[203] However, making regularly patterned surfaces exhibiting self-healing capabilities still needs further research.

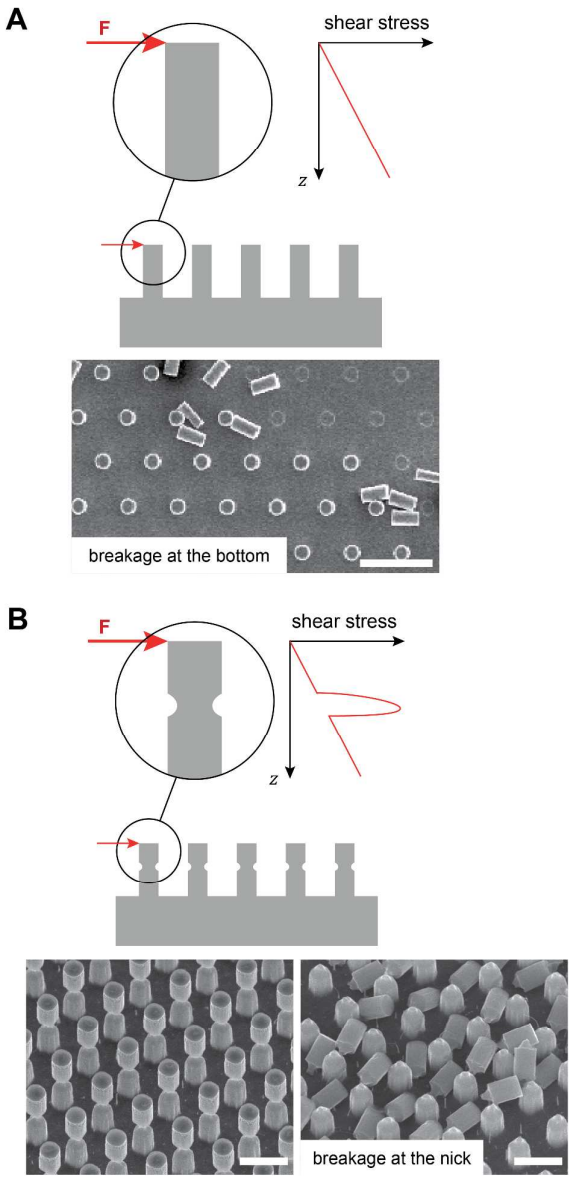

Figure 17. **Mechanical stability to resist shear loads, F, of submicron pillar structures. (A)** Schematic illustration of increasing shear stress that has its maximum value at the substrate when the pillar has a constant cross-sectional area. Micrograph represents intact and pillars upon breakage. Scale bar: 20 μm. **(B)** Schematic illustration of a peak stress at the tapered, overhanging part of the pillar. Micrographs represent intact (left) and pillars upon breakage (right). Scale bars: 4 μm. Adapted from Ref. Hensel[204].

5. Synthetic omniphobic surfaces and their applications

The recently achieved insights into the fundamentals of omniphobicity inspired scientists to fabricate synthetic omniphobic surfaces. Most of the applications were already tackled using bio-inspired superhydrophobic surfaces; however, the geometrical concept of designing omniphobic surfaces has the potential to improve or even expand the areas of application.

5.1. Self-cleaning and easy-to-clean surfaces

Particularly inspired by the hierarchical structure of the lotus leaf, several approaches for artificial self-cleaning surfaces have been proposed over the last two decades. Dust particles can be easily carried away by sliding water droplets due to their higher affinity to the water-air interface than to the rough solid surface. However, low-surface-tension liquids such as oils or aqueous media contaminated by surfactants are usually able to wet those surfaces and diminish the self-cleaning capability. To overcome this limitation, omniphobic surfaces play a crucial role. In particular, super-omniphobic surfaces, which exhibit high contact angle and low contact angle hysteresis for both water and oil, have excellent self-cleaning capabilities. Back in 1997, the first reported omniphobic surface exhibited high contact angles for low-surface-tension liquids.[86] More recently, Kim *et al*. reported on self-cleaning using glycerin to remove aluminum hydroxide particles adsorbed to an omniphobic silicon surface made by chemical wet etching.[205] Yuan and Jin reported on the fabrication of self-assembled, hierarchical, silica nanowire-based surfaces and demonstrated the cleaning capabilities by removing forcibly formed dirt spots using water.[206] Zhao and Law investigated the anisotropic self-cleaning capabilities on grooved surfaces that exhibit different wetting characteristics parallel and perpendicular to the spatial orientation of the grooves.[207] Thus, droplet advancement carrying dust particles from the surface could be directed, similar to the anisotropic wetting behavior of butterfly wings or rice leaves.[208,209]

Besides removing dust particles, the prevention of fingerprints on finger-touch controlled devices such as mobile phones or tablet computers represents a current challenge in fabricating omniphobic surfaces. Residual fingerprints reduce the gloss on screens and therefore the perfect visual appearance. Furthermore, the residues can be misused to attack the devices by reading-out the password.[210] Recently, Siriviriyanun and Imae proposed the utilization of oleic acid, the main component of a fingerprint, to evaluate the anti-fingerprint characteristics.[211] They could further demonstrate that a purely chemical surface modification using self-assembled methyl terminated organosiloxane coatings provide higher contact angles for oleic acid in comparison with untreated surfaces and, therefore, better anti-fingerprint properties. Nowadays, a solely chemical surface modification cannot prevent the deposition of fingerprints on screen or glasses, but provide easy-to-clean surfaces that can be cleaned by wiping with soft cloth.[212] To further integrate true oil-repellence in such devices, the future challenge comprises the development of transparent, but also rough super-omniphobic surfaces exhibiting cross-sectional profiles with overhangs in combination with sufficient high mechanical durability.

5.2. Chemical shielding and non-fouling characteristics

The ability of omniphobic surfaces to repel various liquids can protect devices against several chemicals such as Newtonian and non-Newtonian liquids.[213] Omniphobic coatings furthermore provide the ability to delay or to prevent corrosion of metals such as copper, iron, or aluminum upon immersion into concentrated acids or bases due to the reduced or hindered contact of the corrosive media with the metal.[213,214] For biomedical applications, such coatings can reduce the adsorption of proteins or blood cells that may prevent the clogging of synthetic materials coming into contact with human blood. Paven *et al*. reported on the modification of macroporous membranes with a super-omniphobic layer for a potential application in carbon dioxide capture and heart-lung machines.[215] The fractal-like network of fluorinated silica particles could efficiently inhibit the adsorption of proteins even upon 24 h exposure. The geometrical concept of omniphobic surfaces, which often exhibit surface features in the sub-micron range, has indeed high potential to control or even prevent the biofilm formation that includes the settling and colonialization of bacteria onto the surface. Hochbaum and Aizenberg demonstrated the bacterial ordering and oriented attachment on the single-cell level as induced by nanometer-scale periodic surface features.[216] However to control the overall biofilm formation process, the adsorption of proteins is nonetheless essential as it is typically the first step in biofilm formation and depends rather on the surface chemistry.[217]

6. Conclusions and perspectives

Nature has evolved a number of liquid-repellent surfaces that have inspired research towards synthetic surfaces with similar characteristics. Many techniques to fabricate liquid-repellent surfaces have been established;[16,18,43,101,218] however, most of them are limited to the laboratory and cannot be transferred to industrial-scale manufacturing processes. The durability, which is mainly restricted by the mechanical resistance, is a further critical point in the implementation of omniphobic surfaces into every day products. To overcome this problem, more research on novel concepts of structural designs is required.

In this article, several examples of water and oil-repellent natural surfaces were briefly summarized. Emphasis was put on the cuticular structures found on springtails, which exhibit omniphobic wetting characteristics to ensure survival in temporarily rain-flooded soil habitats. A most striking feature of collembolan cuticle is the hierarchically arranged and highly textured surface that covers the entire body of the animal: Nanoscopic primary granules that are interconnected by ridges and together form a unique comb structure. It was shown that the presence of overhanging cross-sections allowed for omniphobicity. A high-pressure resistance against complete wetting could be obtained by abstraction of the skin morphology into serif T structures and miniaturization of the surface features, irrespective of the surface chemistry. In addition, the hierarchically assembled surface enables a reversible partial wetting because nanoplastrons remain stuck inside the nanocavities, which facilitates recovery of the dewetted state upon pressure reduction. Transferring the springtail-inspired comb pattern into polymer membranes with individual cavities enhanced the mechanical stability compared with an array of single pillars made of the same material. Accordingly, a broad spectrum of emerging applications may benefit, including products requiring self-cleaning, anti-fingerprint, and anti-corrosion coatings and the prevention of bio-fouling.

In particular, the fact that the surface chemistry does not influence the resistance against complete wetting, when using the appropriate structural design, permits the preparation of omniphobic surfaces that, in turn, can be optimized by tailoring the surface chemistry. Thus,

synthetic liquid-repellent surfaces are no longer restricted to fluorine-based coatings in accordance with natural surfaces. Grafting to or grafting from the asperities using selected agents may be utilized to comply with further practical challenges such as anti-icing or optical properties. Furthermore, attaching stimuli-responsive molecules to omniphobic surfaces can be expected to pave the way for additional exciting advancements in switchable materials.

Acknowledgements

The authors gratefully acknowledge valuable input by Ralf Helbig and Julia Nickerl (both IPF Dresden); many of the reported findings about springtail cuticles were obtained within their thesis projects. C.W. received funding by the German Research Foundation (Deutsche Forschungsgemeinschaft) through the grant "Mechanically stable anti-adhesive polymer surfaces through biomimetic patterning". R.H. acknowledges partial funding from the European Research Council under the European Union's Seventh Framework Program (FP/2007-2013)/ERC Advanced Grant n. 340929.

References

1 F. Xia, L. Jiang and B. F. Xia, *Adv. Mater.*, 2008, **20**, 2842–2858.
2 T. Sun, L. Feng, X. Gao and L. Jiang, *Acc. Chem. Res.*, 2005, **38**, 644–652.
3 B. Bhushan, Y. C. Jung and K. Koch, *Philos. Trans. A. Math. Phys. Eng. Sci.*, 2009, **367**, 1631–72.
4 P. Fratzl and R. Weinkamer, *Prog. Mater. Sci.*, 2007, **52**, 1263–1334.
5 K. Koch, B. Bhushan and W. Barthlott, *Soft Matter*, 2008, **4**, 1943.
6 S. N. Gorb, *Functional surfaces in biology*, Springer, 2009, vol. 2.
7 T. Darmanin and F. Guittard, *Mater. Today*, 2015, **18**, 273–285.
8 R. Jelinek, *Biomimetics: A molecular perspective*, Walter de Gruyter, 2013.
9 E. Dujardin and S. Mann, *Adv. Mater.*, 2002, **14**, 775.
10 B. Bhushan, *Langmuir*, 2012, **28**, 1698–1714.
11 X. Y. Liu, *Bioinspiration: From Nano to Micro Scales*, Springer, 2012.
12 K. Liu and L. Jiang, *Nano Today*, 2011, **6**, 155–175.
13 P. Y. Chen, J. McKittrick and M. A. Meyers, *Prog. Mater. Sci.*, 2012, **57**, 1492–1704.
14 M. A. Meyers, P.-Y. Chen, A. Y.-M. Lin and Y. Seki, *Prog. Mater. Sci.*, 2008, **53**, 1–206.
15 F. T. Malik, R. M. Clement, D. T. Gethin, W. Krawszik and a R. Parker, *Bioinspir. Biomim.*, 2014, **9**, 031002.
16 Y. Y. Yan, N. Gao and W. Barthlott, *Adv. Colloid Interface Sci.*, 2011, **169**, 80–105.
17 T.-S. Wong, T. Sun, L. Feng and J. Aizenberg, *MRS Bull.*, 2013, **38**, 366–371.
18 L. Yao and J. He, *Prog. Mater. Sci.*, 2014, **61**, 94–143.
19 M. Nosonovsky and B. Bhushan, *Curr. Opin. Colloid Interface Sci.*, 2009, **14**, 270–280.
20 Z. Guo, W. Liu and B. L. Su, *J. Colloid Interface Sci.*, 2011, **353**, 335–355.
21 K. Koch, B. Bhushan and W. Barthlott, *Prog. Mater. Sci.*, 2009, **54**, 137–178.
22 C. Neinhuis and W. Barthlott, *Ann. Bot.*, 1997, **79**, 667–677.
23 W. Barthlott and C. Neinhuis, *Planta*, 1997, **202**, 1–8.
24 W. Barthlott and N. Ehler, *Trop. Subtrop. Pflanzenwelt*, 1977, **19**, 367–465.
25 W. Barthlott and E. Wollenweber, *Trop. Subtrop. Pflanzenwelt*, 1981, **32**, 67.
26 T. C. Hobæk, K. G. Leinan, H. P. Leinaas and C. Thaulow, *Bionanoscience*, 2011, **1**, 63–77.
27 J. W. Bush and D. L. Hu, *Annu. Rev. Fluid Mech.*, 2006, **38**, 339–369.
28 J. W. M. Bush, D. L. Hu and M. Prakash, *Adv. In Insect Phys.*, 2007, **34**, 117–192.
29 X.-Q. Feng, X. Gao, Z. Wu, L. Jiang and Q.-S. Zheng, *Langmuir*, 2007, **23**, 4892–6.
30 P. J. Wei, Y. X. Shen and J. F. Lin, *Langmuir*, 2009, **25**, 7006–7009.
31 D. L. Hu, B. Chan and J. W. M. Bush, *Nature*, 2003, **424**, 663–666.

32 D. L. Hu and J. W. M. Bush, *J. Fluid Mech.*, 2010, **644**, 5.
33 M. Prakash and J. W. M. Bush, *Int. J. Non. Linear. Mech.*, 2011, **46**, 607–615.
34 M. T. Marx and B. Messner, *Org. Divers. Evol.*, 2012, **12**, 403–408.
35 T. Pfingstl and G. Krisper, *Zoomorphology*, 2014, **133**, 359–378.
36 D. Neumann and D. Woermann, *Naturwissenschaften*, 2009, **96**, 933–941.
37 W. H. Thorpe and D. J. Crisp, *J. Exp. Biol.*, 1947, **24**, 227–269.
38 C. a. Brewer, W. K. Smith and T. C. Vogelmann, *Plant, Cell Environ.*, 1991, **14**, 955–962.
39 M. R. Flynn and J. W. M. Bush, *J. Fluid Mech.*, 2008, **608**, 275–296.
40 R. S. Seymour and S. K. Hetz, *J. Exp. Biol.*, 2011, **214**, 2175–2181.
41 VDI, *Biomimetics. Conception and strategy. Differences between bionic and conventional methods/products.*, VDI-Richtlinien. Berlin: Beuth., 2011.
42 M. Ma and R. M. Hill, *Curr. Opin. Colloid Interface Sci.*, 2006, **11**, 193–202.
43 T. Darmanin, E. Taffin de Givenchy, S. Amigoni and F. Guittard, *Adv. Mater.*, 2013, **25**, 1378–94.
44 E. Celia, T. Darmanin, E. Taffin de Givenchy, S. Amigoni and F. Guittard, *J. Colloid Interface Sci.*, 2013, **402**, 1–18.
45 L. Feng, S. H. Li, Y. S. Li, H. J. Li, L. J. Zhang, J. Zhai, Y. L. Song, B. Q. Liu, L. Jiang and D. B. Zhu, *Adv. Mater.*, 2002, **14**, 1857–1860.
46 P. Wagner, R. Fürstner, W. Barthlott and C. Neinhuis, *J. Exp. Bot.*, 2003, **54**, 1295–1303.
47 B. Bhushan and Y. C. Jung, *Prog. Mater. Sci.*, 2011, **56**, 1–108.
48 K. S. Liu, Y. Tian and L. Jiang, *Prog. Mater. Sci.*, 2013, **58**, 503–564.
49 A. Solga, Z. Cerman, B. F. Striffler, M. Spaeth and W. Barthlott, *Bioinspir. Biomim.*, 2007, **2**, S126–S134.
50 Q.-S. Zheng, Y. Yu and Z.-H. Zhao, *Langmuir*, 2005, **21**, 12207–12212.
51 H. Zhao, K.-C. Park and K.-Y. Law, *Langmuir*, 2012, **28**, 14925–14934.
52 T. Verho, C. Bower, P. Andrew, S. Franssila, O. Ikkala and R. H. A. Ras, *Adv. Mater.*, 2011, **23**, 673–678.
53 E. Huovinen, J. Hirvi, M. Suvanto and T. A. Pakkanen, *Langmuir*, 2012, **28**, 14747–14755.
54 D. Quéré and M. Reyssat, *Philos. Trans. R. Soc. A Math. Phys. Eng. Sci.*, 2008, **366**, 1539–1556.
55 A. Tuteja, W. Choi, G. H. McKinley, R. E. Cohen and M. F. Rubner, *MRS Bull.*, 2008, **33**, 752–758.
56 L. Cao, H.-H. A. Hu and D. Gao, *Langmuir*, 2007, **23**, 4310–4314.
57 N. A. Patankar, *Langmuir*, 2004, **20**, 7097–7102.
58 N. A. Patankar, *Langmuir*, 2003, **19**, 1249–1253.
59 X. Feng and L. Jiang, *Adv. Mater.*, 2006, **18**, 3063–3078.
60 M. J. Hancock, K. Sekeroglu and M. C. Demirel, *Adv. Funct. Mater.*, 2012, **22**, 2223–2234.
61 H.-J. Butt, C. Semprebon, P. Papadopoulos, D. Vollmer, M. Brinkmann and M. Ciccotti, *Soft Matter*, 2013, **9**, 418.
62 H.-J. Butt, I. V Roisman, M. Brinkmann, P. Papadopoulos, D. Vollmer and C. Semprebon, *Curr. Opin. Colloid Interface Sci.*, 2014, **19**, 343–354.
63 A. K. Kota, G. Kwon and A. Tuteja, *NPG Asia Mater.*, 2014, **6**, e109.
64 A. Cavalli, P. Bøggild and F. Okkels, *Langmuir*, 2012, **28**, 17545–51.
65 A. Cavalli, P. Bøggild and F. Okkels, *Soft Matter*, 2013, **9**, 2234–2238.
66 C.-H. Choi and C.-J. Kim, *Phys. Rev. Lett.*, 2006, **96**, 066001.
67 Y. Rahmawan, L. Xu and S. Yang, *J. Mater. Chem. A*, 2013, **1**, 2955.
68 X. Deng, L. Mammen, H.-J. Butt and D. Vollmer, *Science (80-.).*, 2012, **335**, 67–70.
69 W. Li, G. Fang, Y. Li and G. Qiao, *J. Phys. Chem. B*, 2008, **112**, 7234–7243.
70 S. Jung, M. Dorrestijn, D. Raps, A. Das, C. M. Megaridis and D. Poulikakos, *Langmuir*, 2011, **27**, 3059–3066.
71 A. Sidorenko, T. Krupenkin and J. Aizenberg, *J. Mater. Chem.*, 2008, **18**, 3841.

72 R. Wang, K. Hashimoto, A. Fujishima, M. Chikuni, E. Kojima, A. Kitamura, M. Shimohigoshi and T. Watanabe, *Nature*, 1997, **388**, 431–432.
73 Q. Cheng, M. Li, Y. Zheng, B. Su, S. Wang and L. Jiang, *Soft Matter*, 2011, **7**, 5948.
74 J.-H. Kang, Y.-J. Lee, B.-K. Oh, S.-K. Lee, B.-R. Hyun, B.-W. Lee, Y.-G. Choi, K.-S. Nam and J.-D. Lim, *J. Asia-Pacific Biodivers.*, 2014, **7**, 484–488.
75 P. G. De Gennes, *Rev. Mod. Phys.*, 1985, **57**, 827–863.
76 T. Young, *Philos. Trans. R. Soc. London*, 1805, **95**, 65–87.
77 P. S. Laplace, *Mécanique céleste. Suppl. au Xieme Livre*, Lourier, Paris, 1805.
78 S. D. Poisson, *Nouvelle Théorie de L'action Capillaire*, Bochelier, Paris, 1831.
79 D. H. Andrews, *The collected works of J. Willard Gibbs*, Yale University Press, London, 1957.
80 R. N. Wenzel, *Ind. Eng. Chem. Res.*, 1936, **28**, 988–994.
81 B. D. Cassie, A. B. D. Cassie and S. Baxter, *Trans. Faraday Soc.*, 1944, **40**, 546–551.
82 A. Lafuma and D. Quéré, *Nat. Mater.*, 2003, **2**, 457–460.
83 A. Marmur, *Langmuir*, 2003, **19**, 8343–8348.
84 J. Drelich and A. Marmur, *Surf. Innov.*, 2013, **2**, 211–227.
85 A. Marmur, *Langmuir*, 2008, **24**, 7573–9.
86 K. Tsujii, T. Yamamoto, T. Onda and S. Shibuichi, *Angew. Chemie Int. Ed. English*, 1997, **36**, 1011–1012.
87 H. Search, C. Journals, A. Contact, M. Iopscience, I. P. Address and S. Herminghaus, *Europhys. Lett.*, 2000, **52**, 165–170.
88 J.-L. Liu, X.-Q. Feng, G. Wang and S.-W. Yu, *J. Phys. Condens. Matter*, 2007, **19**, 356002.
89 N. A. Patankar, *J. Adhes. Sci. Technol.*, 2009, **23**, 413–433.
90 M. E. Abdelsalam, P. N. Bartlett, T. Kelf and J. Baumberg, *Langmuir*, 2005, **21**, 1753–7.
91 A. Starostin, V. Valtsifer, V. Strelnikov, E. Bormashenko, R. Grynyov, Y. Bormashenko and A. Gladkikh, *Adv. Eng. Mater.*, 2014, **16**, 1127–1132.
92 W. Dong, Y. Zhou, D. Yan, Y. Mai, L. He and C. Jin, *Langmuir*, 2009, **25**, 173–178.
93 T. Darmanin and F. Guittard, *Prog. Polym. Sci.*, 2014, **39**, 656–682.
94 S. M. M. Ramos, A. Benyagoub, B. Canut and C. C. Jamois, *Langmuir*, 2010, **26**, 5141–5146.
95 W. Choi, A. Tuteja, S. S. Chhatre, J. M. Mabry, C. R., R. E. Cohen and G. H. McKinley, *Adv. Mater.*, 2009, **21**, 2190–2195.
96 T. Darmanin, J. Tarrade, E. Celia and F. Guittard, *J. Phys. Chem. C*, 2014, **118**, 2052–2057.
97 A. Tuteja, W. Choi, M. L. Ma, J. M. Mabry, M. S., G. C. Rutledge, G. H. McKinley, R. E. Cohen and S. a Mazzella, *Science (80-.).*, 2007, **318**, 1618–1622.
98 A. Tuteja, W. Choi, J. M. Mabry, G. H. McKinley and R. E. Cohen, *Proc. Natl. Acad. Sci. U. S. A.*, 2008, **105**, 18200–5.
99 R. Dufour, M. Harnois, Y. Coffinier, V. Thomy, R. Boukherroub and V. Senez, *Langmuir*, 2010, **26**, 17242–17247.
100 T. P. N. Nguyen, R. Boukherroub, V. Thomy and Y. Coffinier, *J. Colloid Interface Sci.*, 2014, **416**, 280–288.
101 T. Jiang, Z. Guo and W. Liu, *J. Mater. Chem. A*, 2015, **3**, 1811–1827.
102 A. K. Kota, J. M. Mabry and A. Tuteja, *Surf. Innov.*, 2013, **1**, 71–83.
103 R. Helbig, J. Nickerl, C. Neinhuis and C. Werner, *PLoS One*, 2011, **6**, e25105.
104 R. Hensel, R. Helbig, S. Aland, H. G. Braun, A. Voigt, C. Neinhuis and C. Werner, *Langmuir*, 2013, **29**, 1100–1112.
105 R. Hensel, R. Helbig, S. Aland, A. Voigt, C. Neinhuis and C. Werner, *NPG Asia Mater.*, 2013, **5**, e37.
106 A. K. Epstein, B. Pokroy, A. Seminara and J. Aizenberg, *Proc. Natl. Acad. Sci. U. S. A.*, 2011, **108**, 995–1000.
107 R. Rakitov and S. N. Gorb, *Proc. R. Soc. B Biol. Sci.*, 2013, **280**, 20122391.
108 T.-S. Wong, S. H. Kang, S. K. Y. Tang, E. J. Smythe, B. D. Hatton, A. Grinthal and J. Aizenberg, *Nature*, 2011, 477, 443–447.

109 N. Vogel, R. a Belisle, B. Hatton, T.-S. Wong and J. Aizenberg, *Nat. Commun.*, 2013, **4**, 2167.
110 A. K. Epstein, T.-S. Wong, R. A. Belisle, E. M. Boggs and J. Aizenberg, *Proc. Natl. Acad. Sci.*, 2012, **109**, 13182–13187.
111 P. Kim, T. S. Wong, J. Alvarenga, M. J. Kreder, W. E. Adorno-Martinez and J. Aizenberg, *ACS Nano*, 2012, **6**, 6569–6577.
112 H.-J. Schulz, in *Exkursionsfauna von Deutschland, Band 2, Wirbellose Insekten*, ed. B. Klausnitzer, Spektrum Akademischer Verlag, Heidelberg, 11th edn., 2011, pp. 45–53.
113 S. P. Hopkin, *Biology of the springtails (Insecta: Collembola)*, Oxford University Press, USA, 1997.
114 P. F. Bellinger, K. A. Christiansen and F. Janssens, *Checkl. Collembola World*, http://www.collembola.org, Accessed: May 12, 2015.
115 K. Meusemann, B. M. von Reumont, S. Simon, F. Roeding, S. Strauss, P. Kuck, I. Ebersberger, M. Walzl, G. Pass, S. Breuers, V. Achter, A. von Haeseler, T. Burmester, H. Hadrys, J. W. Wagele, B. Misof, P. Kück and J. W. Wägele, *Mol. Biol. Evol.*, 2010, **27**, 2451–2464.
116 F. Nardi, G. Spinsanti, J. L. Boore, A. Carapelli, R. Dallai and F. Frati, *Science (80-.).*, 2003, **299**, 1887–1889.
117 S. Hirst and S. Maulik, *Geol. Mag.*, 1926, **63**, 69.
118 P. Whalley and E. A. Jarzembowski, *Nature*, 1981, **291**, 317–317.
119 D. A. Grimaldi, *Arthropod Struct. Dev.*, 2010, **39**, 191–203.
120 R. Jordana, E. Baquero, S. Reboleira and A. Sendra, *Terr. Arthropod Rev.*, 2012, **5**, 35–85.
121 R. H. Brand, *Am. Midl. Nat.*, 2002, **148**, 383.
122 M. A. Elnitsky, J. B. Benoit, D. L. Denlinger and R. E. Lee, *J. Insect Physiol.*, 2008, **54**, 1432–1439.
123 P. Greenslade, *J. Arid Environ.*, 1980, **4**, 219–228.
124 N. M. Teets and D. L. Denlinger, *J. Exp. Biol.*, 2014, **217**, 84–93.
125 L. Cheng, *Marine insects*, North-Holland Publishing Company, 1976.
126 J. Rusek, *Biodivers. Conserv.*, 1998, **7**, 1207–1219.
127 A. Milcu, S. Partsch, R. Langel and S. Scheu, *Oikos*, 2006, **112**, 513–524.
128 W. M. Davies, *Q. J. Microsc. Sci.*, 1927, **71**, 15–30.
129 D. Zinkler, *Z. Vgl. Physiol.*, 1966, **52**, 99–144.
130 J. Nickerl, R. Helbig, H. J. Schulz, C. Werner and C. Neinhuis, *Zoomorphology*, 2013, **132**, 183–195.
131 H. Gundersen, H. P. Leinaas and C. Thaulow, *PLoS One*, 2014, **9**, e86783.
132 W. H. Thorpe, *Biol. Rev.*, 1950, **25**, 344–390.
133 H. Gundersen, C. Thaulow and H. P. Leinaas, *Zoomorphology*, 2015, **134**, 211–218.
134 P. D. Moore, *Nature*, 2002, **418**, 381.
135 S. Fridriksson, *Surtsey: Evolution of life on a volcanic island*, Elsevier, 2013.
136 D. L. Hu and J. W. M. Bush, *Nature*, 2005, **437**, 733–736.
137 D. L. Hu, M. Prakash, B. Chan and J. W. M. Bush, *Exp. Fluids*, 2007, **43**, 769–778.
138 J. Noble-Nesbitt, *J. Exp. Biol.*, 1963, **40**, 681–700.
139 L. Deharveng, C. A. D'Haese and A. Bedos, *Hydrobiologia*, 2008, **595**, 329–338.
140 A. D. Imms, *L.M.B.C. Memoirs on Typical British Marine Plants and Animals*, Liverpool Marine Biology Committee, 1906, vol. 13. Anurid.
141 F. Brocher, *Ann. Biol. Lacustre*, 1910, **4**, 89–138.
142 H. E. Hinton, *Annu. Rev. Entomol.*, 1969, **14**, 343–368.
143 J. Noble-Nesbitt, *Q. J. Microsc. Sci.*, 1963, **3**, 253–270.
144 P. N. Lawrence and Z. Massoud, *Rev. Ecol. Biol. Sol*, 1973, **10**, 77–101.
145 W. G. Hale and A. L. Smith, *Rev. d'Ecologie Biol. du Sol*, 1966, **52**, 343–354.
146 R. Hensel, A. Finn, R. Helbig, S. Killge, H.-G. Braun and C. Werner, *Langmuir*, 2014, **30**, 15162–15170.
147 H. Ghiradella and W. Radigan, *J. Insect Physiol.*, 1974, **20**, 301–306.
148 M. T. Marx, P. Guhmann and P. Decker, *Animals*, 2012, **2**, 564–590.

149 P. E. King, P. J. A. Pugh, M. R. Fordy, N. Love and S. A. Wheeler, *J. Nat. Hist.*, 1990, **24**, 673–688.
150 H. Ghiradella, *Adv. In Insect Phys.*, 2010, **38**, 135–180.
151 A. C. Neville, *Biology of the arthropod cuticle*, Springer-Verlag, Berlin, 4th edn., 1975.
152 J. Nickerl, M. Tsurkan, R. Hensel, C. Neinhuis and C. Werner, *J. R. Soc. Interface*, 2014, **11**, 20140619.
153 L. McGaw, A. Jäger and J. Van Staden, *South African J. Bot.*, 2002, **68**, 417–423.
154 K. Benkendorff, A. R. Davis, C. N. Rogers and J. B. Bremner, *J. Exp. Mar. Bio. Ecol.*, 2005, **316**, 29–44.
155 A. P. Desbois and V. J. Smith, *Appl. Microbiol. Biotechnol.*, 2010, **85**, 1629–1642.
156 J. Gershenzon and N. Dudareva, *Nat. Chem. Biol.*, 2007, **3**, 408–414.
157 S. Ögel, *Comm. Fac. Sci. Univ. Ankara*, 1965, **10**, 1–34.
158 E. N. G. Joosse and E. Veltkamp, *Netherlands J. Zool.*, 1969, **20**, 315–328.
159 J. Noble-Nesbitt, *Q. J. Microsc. Sci.*, 1963, **3**, 369–391.
160 V. B. Wigglesworth, *J. Insect Physiol.*, 1990, **36**, 307–313.
161 J. Francois, D. Herbage and S. Junqua, *Eur. J. Biochem.*, 1980, **112**, 389–396.
162 K. Bailey and T. Weis-Fogh, *Biochim. Biophys. Acta*, 1961, **48**, 452–459.
163 B. Lotz and F. Colonna Cesari, *Biochimie*, 1979, **61**, 205–214.
164 E. S. Lintz and T. R. Scheibel, *Adv. Funct. Mater.*, 2013, **23**, 4467–4482.
165 S. S. Williams, S. Retterer, R. Lopez, R. Ruiz, E. T. Samulski and J. M. DeSimone, *Nano Lett.*, 2010, **10**, 1421–1428.
166 D. Bonn, *Curr. Opin. Colloid Interface Sci.*, 2001, **6**, 22–27.
167 E. Bormashenko, in *Encyclopedia of Nanotechnology*, Springer, 2012, pp. 2830–2837.
168 D. Quéré, *Annu. Rev. Mater. Res.*, 2008, **38**, 71–99.
169 C. Ishino, K. Okumura and D. Quéré, *Europhys. Lett.*, 2007, **68**, 419–425.
170 A. Marmur, *Annu. Rev. Mater. Res.*, 2009, **39**, 473–489.
171 E. Bormashenko, *Adv. Colloid Interface Sci.*, 2014, DOI:10.1016/j.cis.2014.02.009.
172 D. Soto, A. B. De Larivière, X. Boutillon, C. Clanet and D. Quéré, *Soft Matter*, 2014, **10**, 4929–4934.
173 C. Lee, Y. Nam, H. Lastakowski, J. I. Hur, S. Shin, A.-L. Biance, C. Pirat and C. Ybert, *Soft Matter*, 2015, DOI: 10.1039/C5SM00825E.
174 G. S. Watson, M. Gellender and J. a Watson, *Biofouling*, 2014, 1–8.
175 G. S. Watson, L. Schwarzkopf, B. W. Cribb, S. Myhra, M. Gellender and J. A. Watson, *J. R. Soc. Interface*, 2015, **12**, 20141396.
176 P. Papadopoulos, L. Mammen, X. Deng, D. Vollmer and H. Butt, *Proc. Natl. Acad. Sci. U. S. A.*, 2013, **110**, 3254–3258.
177 V. Senez, V. Thomy and R. Dufour, *Nanotechnologies for Synthetic Super Non-wetting Surfaces*, John Wiley & Sons, 2014.
178 G. Pashos, G. Kokkoris and A. G. Boudouvis, *Langmuir*, 2015, **31**, 3059–3068.
179 W. Ren, *Langmuir*, 2014, **30**, 2879–2885.
180 E. S. Savoy and F. A. Escobedo, *Langmuir*, 2012, **28**, 16080–16090.
181 G. Whyman and E. Bormashenko, *Langmuir*, 2011, **27**, 8171–8176.
182 T. Liu and C. J. Kim, *Sci. (New York, NY)*, 2014, **346**, 1096–1100.
183 A. Jantschke, C. Fischer, R. Hensel, H.-G. Braun and E. Brunner, *Nanoscale*, 2014, **6**, 11637–11645.
184 A. J. B. Milne, J. A. W. Elliott, P. Zabeti, J. Zhou and A. Amirfazli, *Phys. Chem. Chem. Phys.*, 2011, **13**, 16208–16219.
185 X. Wang, L. Chen, E. Bonaccurso and J. Venzmer, *Langmuir*, 2013, **29**, 14855–14864.
186 S. Moulinet and D. Bartolo, *Eur. Phys. J. E*, 2007, **24**, 251–260.
187 C. Antonini, J. B. Lee, T. Maitra, S. Irvine, D. Derome, M. K. Tiwari, J. Carmeliet and D. Poulikakos, *Sci. Rep.*, 2014, **4**, 4055.
188 B. Haimov, S. Pechook, O. Ternyak and B. Pokroy, *J. Phys. Chem. C*, 2013, **117**, 6658–6663.
189 P. Lv, Y. Xue, Y. Shi, H. Lin and H. Duan, *Phys. Rev. Lett.*, 2014, **112**, 196101.

190 E. Søgaard, N. K. Andersen, K. Smistrup, S. T. Larsen, L. Sun and R. Taboryski, *Langmuir*, 2014, **30**, 12960–12968.
191 M. S. Bobji, S. V. Kumar, A. Asthana and R. N. Govardhan, *Langmuir*, 2009, **25**, 12120–12126.
192 L. Lei, H. Li, J. Shi and Y. Chen, *Langmuir*, 2010, **26**, 3666–3669.
193 P. Lv, Y. Xue, H. Liu, Y. Shi, P. Xi, H. Lin and H. Duan, *Langmuir*, 2015, **31**, 1248–1254.
194 T. Verho, J. T. Korhonen, L. Sainiemi, V. Jokinen, C. Bower, K. Franze, S. Franssila, P. Andrew, O. Ikkala and R. H. A. Ras, *Proc. Natl. Acad. Sci. U. S. A.*, 2012, **109**, 10210–3.
195 E. Bormashenko, A. Musin, G. Whyman and M. Zinigrad, *Langmuir*, 2012, **28**, 3460–3464.
196 C. Semprebon, P. Forsberg, C. Priest and M. Brinkmann, *Soft Matter*, 2014, **10**, 5739–48.
197 R. Hensel, A. Finn, R. Helbig, H. G. Braun, C. Neinhuis, W. J. Fischer and C. Werner, *Adv. Mater.*, 2014, **26**, 2029–2033.
198 M. Callies and D. Quéré, *Soft Matter*, 2005, **1**, 55.
199 P. R. Elliott, S. P. Stagon, H. Huang, D. U. Furrer, S. F. Burlatsky and T. P. Filburn, *Sci. Rep.*, 2015, **5**, 9260.
200 A. K. Kota, Y. Li, J. M. Mabry and A. Tuteja, *Adv. Mater.*, 2012, **24**, 5838–43.
201 C. Neinhuis, K. Koch and W. Barthlott, *Planta*, 2001, **213**, 427–434.
202 Y. Li, L. Li and J. Sun, *Angew. Chemie*, 2010, **122**, 6265–6269.
203 H. Jin, X. Tian, O. Ikkala and R. H. A. Ras, *ACS Appl. Mater. Interfaces*, 2013, **5**, 485–488.
204 R. Hensel, *Robust omniphobic surfaces by mimicking the springtail skin morphology*, PhD Thesis, Technische Univeristät Dresden, 2013.
205 T. Il Kim, D. Tahk and H. H. Lee, *Langmuir*, 2009, **25**, 6576–6579.
206 J. J. Yuan and R. H. Jin, *Langmuir*, 2011, **27**, 9588–9596.
207 H. Zhao and K.-Y. Y. Law, *Langmuir*, 2012, **28**, 11812–11818.
208 G. Sun, Y. Fang, Q. Cong and L. Q. Ren, *J. Bionic Eng.*, 2009, **6**, 71–76.
209 D. Wu, J.-N. N. Wang, S.-Z. Z. Wu, Q.-D. D. Chen, S. Zhao, H. Zhang, H.-B. B. Sun and L. Jiang, *Adv. Funct. Mater.*, 2011, **21**, 2927–2932.
210 A. J. Aviv, K. Gibson, E. Mossop, M. Blaze and J. M. Smith, in *WOOT*, 2010, pp. 1–7.
211 A. Siriviriyanun and T. Imae, *Chem. Eng. J.*, 2014, **246**, 254–259.
212 B. Bhushan and P. Muthiah, *Microsyst. Technol.*, 2013, **19**, 1261–1263.
213 S. Pan, A. K. Kota, J. M. Mabry and A. Tuteja, *J. Am. Chem. Soc.*, 2013, **135**, 578–581.
214 B. Ge, Z. Zhang, X. Men, X. Zhu and X. Zhou, *Appl. Surf. Sci.*, 2014, **293**, 271–274.
215 M. Paven, P. Papadopoulos, S. Schöttler, X. Deng, V. Mailänder, D. Vollmer and H.-J. Butt, *Nat. Commun.*, 2013, **4**, 2512.
216 A. I. Hochbaum and J. Aizenberg, *Nano Lett.*, 2010, **10**, 3717–3721.
217 C. M. Kirschner and A. B. Brennan, *Annu. Rev. Mater. Res.*, 2012, **42**, 211–229.
218 H. Bellanger, T. Darmanin, E. Taffin de Givenchy and F. Guittard, *Chem. Rev.*, 2014, **114**, 2694–2716.